

# Analyst

Accepted Manuscript



This is an *Accepted Manuscript*, which has been through the Royal Society of Chemistry peer review process and has been accepted for publication.

*Accepted Manuscripts* are published online shortly after acceptance, before technical editing, formatting and proof reading. Using this free service, authors can make their results available to the community, in citable form, before we publish the edited article. We will replace this *Accepted Manuscript* with the edited and formatted *Advance Article* as soon as it is available.

You can find more information about *Accepted Manuscripts* in the [Information for Authors](#).

Please note that technical editing may introduce minor changes to the text and/or graphics, which may alter content. The journal's standard [Terms & Conditions](#) and the [Ethical guidelines](#) still apply. In no event shall the Royal Society of Chemistry be held responsible for any errors or omissions in this *Accepted Manuscript* or any consequences arising from the use of any information it contains.

## ARTICLE

## Plasmon-Enhanced Optical Sensors: A Review

Ming Li<sup>a</sup>, Scott K Cushing<sup>a,b</sup> and Nianqiang Wu<sup>\*a</sup>

Cite this: DOI: 10.1039/x0xx00000x

Received 00th January 2012,

Accepted 00th January 2012

DOI: 10.1039/x0xx00000x

[www.rsc.org/](http://www.rsc.org/)

Surface plasmon resonance (SPR) has found extensive applications in chemi-sensors and biosensors. Plasmons play different roles in different types of optical sensors. SPR transduces a signal in a colorimetric sensor through shift in the spectral position and intensity in response to external stimuli. SPR can also concentrate the incident electromagnetic field in a nanostructure, modulating fluorescence emission and enabling plasmon-enhanced fluorescence to be used for ultrasensitive detection. Furthermore, plasmons have been extensively used for amplifying a Raman signal in a surface-enhanced Raman scattering sensor. This paper presents a review of recent research progress in plasmon-enhanced optical sensing, giving an emphasis on the physical basis of plasmon-enhanced sensors and how these principles guide the design of sensors. In particular, this paper discusses the design strategies for nanomaterials and nanostructures to plasmonically enhance optical sensing signals, also highlighting the applications of plasmon-enhanced optical sensors in health care, homeland security, food safety and environmental monitoring.

## 1. Introduction

Surface plasmon resonance (SPR) refers to the collective oscillations of the conduction electrons in metallic nanostructures.<sup>1</sup> Both the intensity and the position of the SPR strongly depend on the size, shape and composition of the nanostructures, as well as the dielectric properties of the surrounding environment.<sup>2-6</sup> This variety of responsive variables allows for optical sensors to be created using plasmonic metallic nanostructures. Hence plasmon-enhanced optical sensors are finding increasing application in detection of analytes in biomedical diagnosis, home security, food safety and environmental monitoring.<sup>7-10</sup>

SPR occurs in two distinct forms: localized SPR (LSPR) and propagating surface plasmon polaritons (SPPs). LSPR occurs when the dimensions of a metallic nanostructure are less than the wavelength of incident light, leading to collective but non-propagating oscillations of surface electrons in the metallic nanostructure. The LSPR strongly depends on the refractive index of the surrounding medium, providing the basis for colorimetric plasmonic sensors. LSPR also concentrates the incident electromagnetic (EM) field around the nanostructure. The local EM field can influence optical processes such as fluorescence, Raman scattering and infrared absorption, resulting in plasmon-enhanced fluorescence (PEF), surface-enhanced Raman scattering (SERS), and surface-enhanced infrared absorption spectroscopy (SEIAS). The LSPR-associated EM field extends into the surrounding medium (generally ~30 nm) and decays roughly exponentially for a

dipole. In contrast to LSPR, SPPs are the propagating charge oscillations on the surface of thin metal films. SPP cannot be excited by free-space radiation, instead require momentum matching, such as through periodicity in a nanostructure, for resonance excitation. SPP are modulated by the refractive index of the surrounding medium, transducing the sensor's signal. SPP can also play a role in modulating radiation in PEF and SERS. The evanescent EM field of SPP decays with a longer length (generally ~200 nm) than LSPR, allowing the SPP to be modulated by change at distance farther from the nanostructure surface.

By utilizing LSPR and/or SPP, numerous plasmonic metallic nanostructures have already been developed as signal amplifiers and transducers for sensitive optical sensing. This paper will start with a summary of concepts and principles of plasmonics. Next, three principle types of optical sensors built on plasmonic nanostructures will be discussed, including plasmonic sensors, PEF sensors and SERS sensors. The goal of this review is to give a summary of the underlying physics first, and then apply these principles to guide the design of each type of plasmon-enhanced optical sensor. The design strategies which maximize signal transduction and amplification will be discussed. In addition, this paper will highlight the application of plasmon-enhanced optical sensing in chemical detection and *in-vivo* / *in-vitro* biological sensing.

## 2. Basics of surface plasmon resonance

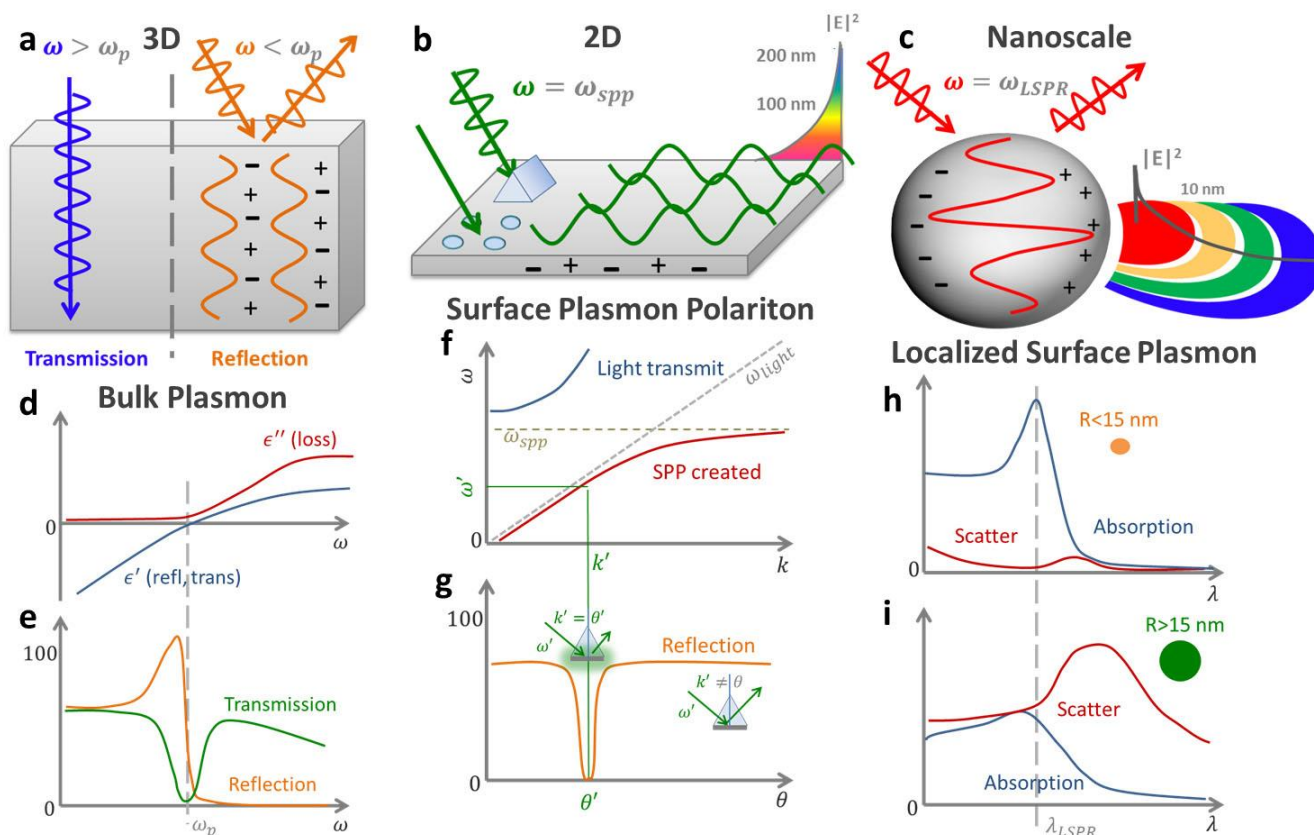


**Figure 1.** Volume, surface and localized surface plasmon resonances. (a) The plasma frequency of a metal describes the frequency below which the conduction electrons oscillate in the incident field. These oscillations lead to a (d) negative real part of the dielectric constant and (e) increased reflection from the metal. (b) On a 2D surface, electron oscillations lead to propagating charge waves known as surface plasmon polaritons (SPPs). These oscillations are coupled to an electromagnetic field which propagates along the interface and with amplitude that exponentially decreases away from the interface. The SPP can only be excited (f) at certain wave vectors and exists as a field that decays evanescently from the surface. The momentum matching condition leads to the SPP resonance (g) only existing at certain incident angles. (c) Localized surface plasmon resonance exists when the metal nanoparticle is smaller than the incident wave length, making the electron oscillations in phase. The collective oscillations lead to a large absorption and scattering cross section, as well as an amplified local EM field. For small particles less than  $\sim 15$  nm, (h) the absorption dominates and the absorption cross-section is large. For big nanoparticles greater than  $\sim 15$  nm, (i) the scattering cross-section dominates. The EM field is taken as polarized in the plane of incidence in the figures.

The free conduction electrons of a metal are influenced by a time-dependent force opposite that of the changing electromagnetic field of the incident light (Figure 1a). The resulting motion of the electrons will be oscillatory, but 180 degrees out of phase due to the charge of the electron, and with dampening caused by Ohmic losses.<sup>11</sup> Like all oscillators, the conduction electrons have a characteristic frequency, in this case known as the plasma frequency<sup>11</sup>

$$\omega_p = \sqrt{\frac{ne^2}{m_{eff}\epsilon_0}} \quad (1)$$

The plasma frequency depends on the density of electrons ( $n$ ) and the effective mass ( $m_{eff}$ ), and corresponds to how easily the electrons can move in response to the incident field. Additionally,  $e$  is the charge of an electron and  $\epsilon_0$  is the permittivity of free space.<sup>11</sup> On average, the free conduction electrons in the bulk of the metal do not oscillate against a

restoring force, so unlike a mass on a spring, there is not a single resonant frequency. Instead the motion is similar to a mass being dragged in a viscous fluid, and will differ based on whether the electrons can respond quickly enough to the driving force of the incident field. If the light has a frequency above the plasma frequency (in the ultraviolet (UV) range for metals), the electrons will not oscillate and the light will simply be transmitted or absorbed in interband transitions.<sup>11</sup> If the light has a frequency smaller than the UV range, the electrons will oscillate 180 degrees out of phase with the incident light, causing a strong reflection.<sup>11</sup> The combination of plasma frequency and interband transitions gives metals their characteristic color. Mathematically this behavior is described by the real part of the dielectric constant ( $\epsilon'_{metal}$ )<sup>12</sup>

$$\frac{\epsilon'_{metal}}{\epsilon_0} = 1 - \left(\frac{\omega_p}{\omega}\right)^2 \quad (2)$$

When the frequency of light is greater than the plasma frequency, the real part of the dielectric constant is positive and

light is transmitted.<sup>12</sup> When the frequency of light is less than the plasma frequency, the

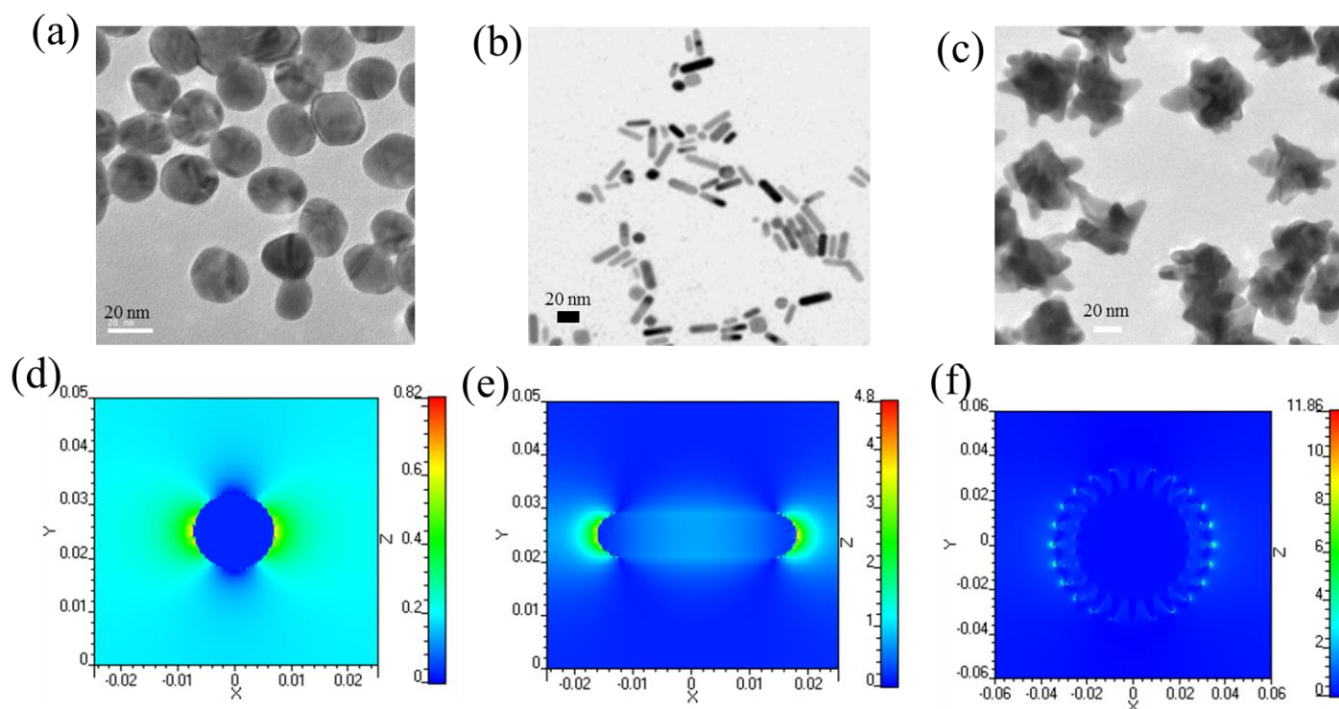


**Figure 2.** TEM images and electric field distributions of (a,d) Au nanosphere, (b,e) Au nanorod and (c,f) Au nanostar synthesized by wet-chemistry methods. (Reprinted with permission from ref. 19, Copyright 2012, IOP Publishing.)

real part of the dielectric constant is negative, and the majority of light is reflected (Figure 1(d, e)).<sup>12</sup> The dielectric constant therefore decides whether or not the metal electrons can oscillate at the given frequency of light. In Figure 1, the convention is used that the positive imaginary part of the dielectric constant corresponds to the Ohmic losses. To avoid confusion, it should be noted that the opposite convention of a negative imaginary part of the dielectric constant referring to loss is also found frequently in literature.

If the bulk metal is now shrunk to a thin film, the oscillations will only exist at the surface, leading to propagating charge waves known as surface plasmon polaritons (SPPs) (Figure 1b).<sup>13,14</sup> The word “polariton” refers to the transformation of the bulk, volume oscillations to travelling surface charge waves. The interface between the metal ( $\epsilon_{\text{metal}}$ ) and the surrounding medium ( $\epsilon_{\text{diel}}$ ) places additional constraints on what frequencies the metal electrons can oscillate in the incident field. This limits the continuous spectrum of Equation 2 (all frequencies below  $\omega_p$ ) for all incident angles to a fixed wave vector and frequency for a given interface. The resulting quantization is why the name is switched from plasma to plasmon.

The resonance condition to excite the SPP is given by<sup>13,14</sup>

$$k_{SPP} = \frac{\omega}{c} \cdot \sqrt{\frac{\epsilon_{\text{metal}} \cdot \epsilon_{\text{diel}}}{\epsilon_{\text{metal}} + \epsilon_{\text{diel}}}}, \quad (3)$$

which gives the dispersion curve for the SPP. The dispersion curve shows the wave vector of light necessary to excite a SPP for a given interface (Figure 1f). The wave vector or momentum of the oscillating charge wave is always greater than that of the massless photon.<sup>13,14</sup> Therefore SPP cannot be directly excited by incident light, but can be only excited by a prism in the Kretschmann geometry, or by a grating to supply the extra momentum.<sup>13</sup> The dispersion curve in Equation 3 gives the angle for which the grating or the prism can supply the necessary momentum to excite the SPP. At this angle, light will be absorbed, leading to a dip in the reflection or transmission spectrum (Figure 1g).

When the metal electrons oscillate, the real part of the dielectric constant is negative, therefore cancel out the denominator in Equation 3, leading to a resonance condition at<sup>13,14</sup>

$$\omega_{SPP} = \frac{\omega_p}{\sqrt{1 + \epsilon_{\text{diel}}}}. \quad (4)$$

The dependence of the SPP frequency on the dielectric constant at the interface transforms the bulk plasma oscillations into a useful transducer for a sensor. The local EM field resulting from the charge oscillations of the SPP extends  $\sim 100$ - $200$  nm into the dielectric.<sup>15</sup> If the local environment changes within this distance, the dielectric constant will differ, and the SPP frequency will shift from that in air. This can be understood conceptually as the dielectric screening the charge at the interface and reducing repulsion between adjacent electrons,

effectively reducing the energy needed to drive oscillations and red-shifting the oscillation frequency. As the SPP frequency changes, so do both the dispersion curve and the angle at which the SPP can be excited, modulating the experimentally measured reflectance. The narrow absorption line shape and high angular specificity of the SPP allow excellent signal-to-noise ratio and figure of merit to be obtained for SPP-based sensors.<sup>13</sup> This sensitivity comes at the trade-off of

experimental simplicity because of the complex geometries needed for detection.<sup>13</sup>

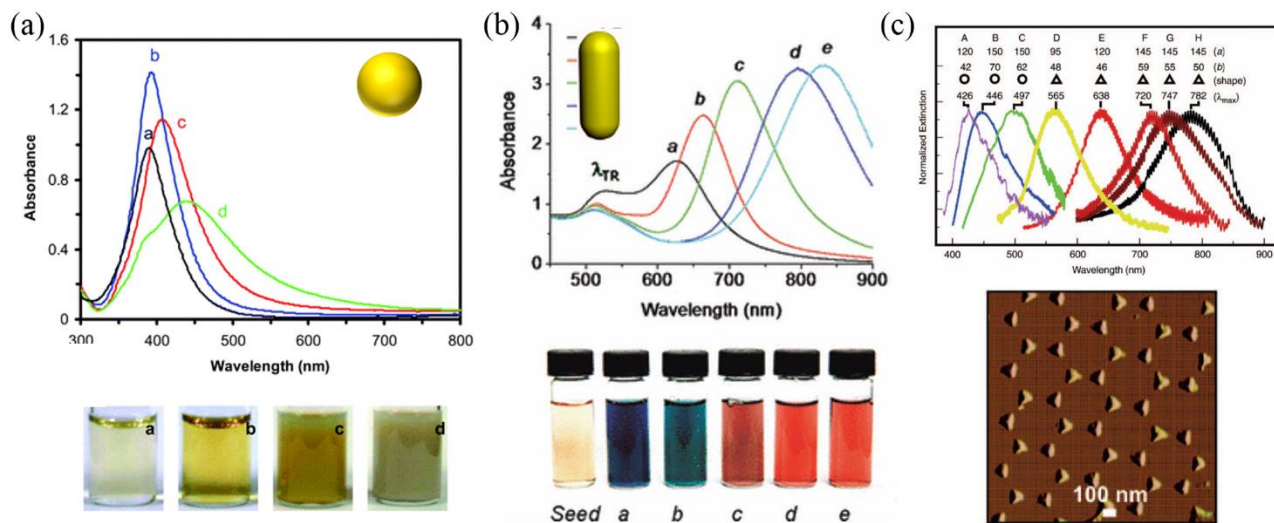


**Figure 3.** Representative plasmonic nanostructures for plasmon-enhanced sensing. (a) Extinction spectra (top), and optical images of different sized Ag nanospheres in aqueous solutions (a:  $3.1 \pm 0.6$  nm, b:  $13.4 \pm 5.8$  nm, c:  $46.4 \pm 6.1$  nm and d:  $91.1 \pm 7.6$  nm. (Reprinted with permission from ref. 22, Copyright 2005, the Royal Society of Chemistry). (b) Extinction spectra (top) and optical images of Au nanorods with various aspect ratios (Reprinted with permission from ref. 23, Copyright 2010, Elsevier B.V.). (c) Size- and shape-tunable localized extinction spectra of various Ag nanosphere and triangle arrays prepared by nanosphere lithography (top), and the representative AFM image of Ag triangle array (Reprinted with permission from ref. 24, Copyright 2005, Materials Research Society).

The restrictions of SPP can be overcome by changing a two-dimensional (2D) metal film to a zero-dimensional (0D) nanoparticle. The incident electric field will be constant across the nanoparticle if it is smaller than the wavelength of light, inducing a uniform displacement of the electron density and a strong restoring force from the positive ionic core background (Figure 1c).<sup>8</sup> The restoring force leads to a characteristic oscillation frequency in the metal electrons similar to a simple harmonic oscillator. This phenomenon is known as LSPR.<sup>8</sup> LSPR can be excited directly by the incident field because the geometry of the nanoparticle supplies the additional momentum.<sup>8</sup> The local environment-induced change in the LSPR peak position can therefore be detected using a simple UV-Visible spectrometer without need of additional gratings or prisms (Figure 1h).

The exact conditions for LSPR can be solved for a nanosphere using Mie theory or a simple harmonic oscillator model,<sup>16-18</sup> as the extinction (absorption + scattering) cross-section is expressed,

$$\sigma_{ext} = 9 \left( \frac{\omega}{c} \right) (\epsilon_{diel})^{\frac{3}{2}} V \frac{\epsilon_{metal}''}{(\epsilon_{metal}' + 2\epsilon_{diel}')^2 + (\epsilon_{metal}'')^2}, \quad (5)$$

Equation 5 shows that when the electrons in the metal oscillate and the real part of the dielectric function is negative, the

denominator will vanish, leading to a strong resonance condition at

$$\omega_{LSPR} = \frac{\omega_p}{\sqrt{1 + 2\epsilon_{diel}'}}, \quad (6)$$

which will shift with change in the local dielectric environment. The coherent oscillations of the electrons make the absorption and scattering cross-section at resonance several orders of magnitude larger than the physical size of the nanoparticle, given by  $V = 4/3\pi R^3$ .

Several key differences exist between LSPR and SPP that must be taken into account when designing a sensor. First, the factor of 2 in front of the interfacial dielectric constant depends on the geometry of the nanoparticle. The LSPR peak position will change with shape in addition to the metal used and the local environment (Figure 2).<sup>19-21</sup> The larger the nanoparticles, the smaller the repulsion for electrons at opposite surfaces, and the more red-shifted the plasmon will be (Figure 3).<sup>22-24</sup> Second, the confined electron oscillations in LSPR lead to an intense local EM field, which can be several orders of magnitude stronger than the incident field strength. In nanoparticles with sharp edges, the field will be concentrated similar to a lightning rod, increasing the local field intensity further and improving the sensitivity to changes in the local environment.<sup>19-21,25,26</sup> The EM field in LSPR decays in  $\sim 10$ - $30$

nm and is therefore more sensitive to changes in distance from the surface of the metal and the local refractive index of the surrounding environment than the SPP that decays in  $\sim 100\text{-}200$  nm.<sup>6,13,18</sup>

Since the LSPR can be excited by incident light, the plasmon can also re-radiate its energy into the far field as scattering, with the size of the particle determining if absorption or scattering dominates (Figure 1(h, i)).<sup>16</sup> In small metal nanoparticles (less than  $\sim 15$  nm) electron-electron scattering quickly converts the energy of the LSPR into heat, which translates into a strong absorption.<sup>8,27,28</sup> In larger particles the electron-electron surface scattering is reduced, and the energy of the plasmons will be re-radiated, leading to a strong scattering cross-section.<sup>8,27,28</sup> The radiative dampening and electron-electron scattering make the lifetime of the LSPR much shorter than that of the SPP.<sup>29</sup> Since the spectral width is inversely related to the lifetime, LSPR has a broader absorption peak than SPP, decreasing the figure of merit of these sensors. The absorption line width can be improved by optimizing the geometry and using planar arrays of metal nanoparticles, decreasing this disadvantage.

Finally, since both SPP and LSPR have local fields, coupling can occur between SPP/SPP, SPP/LSPR, and LSPR/LSPR when the supporting metal structures are brought within the local field decay length.<sup>13</sup> The coupling can lead to an enhanced local field and shifting in the spectral position due to hybridization between the modes.<sup>30</sup> For example, the local field enhancement of two spheres goes from  $\sim 10$  to  $\sim 10^4$  when they are aggregated.<sup>8,13</sup> Shift in the SPP or LSPR frequency can be achieved by aggregating several plasmonic structures upon addition of an analyte, allowing lower detection levels than single particle or film-based designs.

### 3. Plasmonic Sensors

Herein the phrase “plasmonic sensor” refers to sensors that directly utilize shifts in the spectral properties of the plasmon to act as the transducer of the sensing signal. Plasmonic sensors are constructed either with 2D chips that support a SPP mode or with nanoparticles that support LSPR, as mentioned in Section 2.

#### 3.1 Chip-based plasmonic sensors

Planar plasmonic substrates support a propagating SPP mode or a mixed SPP/LSPR mode which can be employed for plasmonic sensing through changes in the refractive index of the surrounding medium. As mentioned in Section 2, SPP can only be excited using a prism or a grating to supply the extra momentum necessary to match to free-space light. The classic setup in chip-based SPP sensors is the Kretschmann configuration (Figure 4),<sup>31</sup> which enables time- and angle-resolved reflectivity measurement of a noble metal film’s SPP mode through a glass prism (typically coated with a  $\sim 40$  nm thick Au film). In this configuration, the metal film is highly reflective except at a specific angle when the SPP is excited, referred to as the SPR angle.<sup>32-36</sup> When molecules (the analyte)

bind to ligands immobilized on the plasmonic metal film, the SPP band red-shifts due to the higher refractive index of the molecules than the aqueous solution, functioning as a sensor.<sup>4,8,37</sup> The wavelength of the SPR peak varies linearly with the refractive index of the surrounding medium according to the Drude model.<sup>12</sup> Hence the refractive index sensitivity ( $S = \Delta\lambda_p / \Delta n$ ) is expressed in units of nm/RIU, where  $\lambda_p$  is the plasmon frequency of the metal and  $n$  is the refractive index of the surrounding medium. A Figure of Merit ( $FOM = S / FWHM$ ) can be defined to evaluate the sensing performance of a plasmonic sensor, where FWHM stands for the full width at half-maxim (that is, the width of SPR peak) and  $S$  is the refractive index sensitivity.

One way to improve the refractive index sensitivity of a plasmonic sensor is to overlap the SPR peak of the metal film with the absorption band of the chromophore that binds to the plasmonic metal.<sup>38,39</sup> Alternatively, the refractive index sensitivity can be improved by replacing the planar metal film with a large-area periodic nano-array pattern such as a nanosphere array, nano-disc array, or nano-triangle array which support both a stronger local EM field and higher sensing area than planar films. Conjugated plasmonic nanoparticles can also be coupled to a Au film in a sandwich configuration when an analyte linker is present, further enhancing the shift of the SPR peak relative to the Au film alone.<sup>40</sup>

The rapid development of nanolithography technology has enabled the controllable fabrication of large-area ( $\sim \text{cm}^2$ ) plasmonic nano-array patterns which combine the advantages of colloidal and planar substrates, including (i) a high density of “hot spots” on the order of a billion or more per  $\text{cm}^2$  with a tunable SPR band and field distribution, resulting in an increased sensitivity compared to a bulk approach,

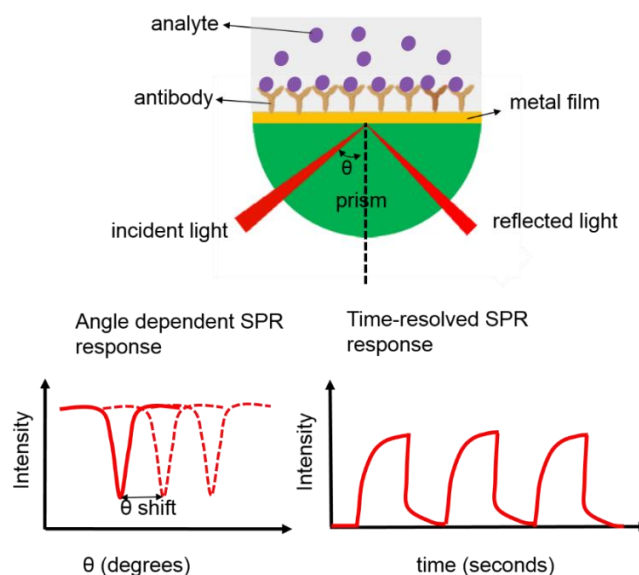


**Figure 4.** Scheme for a plasmonic sensing system based on the Kretschmann configuration. The incident light is reflected by the metal film through a prism, and the reflected beam shows a dark line due to the SPR absorption. This plasmonic sensing system can measure time- and angle-resolved SPR response upon the binding of analytes

(ii) good repeatability, (iii) facile integration with other components (e.g., microfluidics), and (iv) easier accommodation into a portable analytic instrument due to the miniaturized configuration. The nano-hole array is of particular interest to plasmonic sensing. As reported previously,<sup>41</sup> LSPR can occur in an individual nano-hole, leading to a highly concentrated EM field near the edge. When the nano-holes are fabricated periodically over a large-area, SPP can be excited, leading to “extraordinary optical transmission” through the nano-holes at certain resonance wavelengths.<sup>42</sup> The SPP mode is dependent on the periodicity of the nano-hole array. For a non-periodic nano-hole array, the SPP mode disappears while the LSPR mode still exists.<sup>41</sup> The SPP and LSPR modes can be detected directly by incident light without the use of a prism, especially in the case of “extraordinary optical transmission” where front side illumination/back side detection is possible.<sup>41</sup> Periodic structures significantly simplify the configuration of SPP-based sensors, eliminating the typical angle-resolved reflection arrangement used in the Kretschmann configuration, and allowing a nano-hole array-based plasmonic sensor to have a small footprint for miniaturization.

The spectral peaks of the SPP and LSPR in a periodic nano-hole array are highly sensitive to the dielectric properties at the interface, with the adsorption of molecules on the nano-hole leading to a shift in the peaks.<sup>43,44</sup> The plasmonic nano-hole array is particularly suitable for integration into microfluidics,<sup>45</sup> enabling real-time measurement of antibody-ligand binding kinetics<sup>46</sup> and/or multiplexed detection.<sup>47</sup> For example, Pang *et al* demonstrated a high-performance, microfluidic nano-hole array with a refractive index sensitivity of 1520 nm/RIU based on sequential injection of ethylene glycol in water.<sup>48</sup>

Plasmonic chip-based sensors have three distinct advantages:<sup>49-52</sup> (i) label-free detection simplifies the configuration and operation of the sensor, and eliminates the use of multiple antibodies as employed in enzyme-linked immunosorbent assay (ELISA), the gold standard of analytical assays;<sup>49</sup> (ii) real-time measurement of reaction kinetics when the plasmonic chip is integrated into a flow-cell, which provides a powerful tool for studying the binding events;<sup>50,51</sup> and (iii) long-range SPP (LRSP) modes can be formed, which show orders of magnitude less damping than conventional SPP.<sup>52</sup> The smaller damping in LRSP allows narrower bandwidths and higher FOM, as well as a penetration depth of more than 1  $\mu\text{m}$ ,<sup>53</sup> which is ideal for the analysis of living organisms.<sup>54</sup> LRSP modes are possible when a thin metal film is embedded between two dielectrics with similar refractive indices.<sup>55</sup>

### 3.2 Colloidal nanoparticle-based plasmonic sensors

Nanoparticles such as Au, Ag, and Cu exhibit shape- and size-dependent LSPR absorption and scattering bands, which have been utilized to construct plasmonic sensors. There are two types of plasmonic sensors based on the LSPR peak shift: (i) The LSPR peak wavelength shifts when an analyte binds to the nanoparticle's surface, changing the local refractive index;<sup>56</sup> (ii) The plasmonic fields of multiple nanoparticles are coupled

when an analyte brings the nanoparticles into proximity, causing a shift of the LSPR and thereby a color change.<sup>57-60</sup> Among the various plasmonic nanoparticles, colloidal Au nanoparticles are the most commonly used plasmonic transducer because of their chemical stability and visual color change to the naked eye.

Colorimetric detection is a simple and facile method for the detection of analytes in a solution because it provides a direct way to visualize the analyte concentration through the color change. Functionalized Au nanoparticles have been used in colorimetric detection of heavy metals, biological small molecules and biomacromolecules.<sup>61-71</sup> When designing a sensor, surface modification is extremely important since it determines both the sensitivity and selectivity. The Mirkin's group<sup>72</sup> pioneered a colorimetric detection approach in which polynucleotides were selectively detected based on the distance-dependent LSPR coupling between Au nanoparticles.

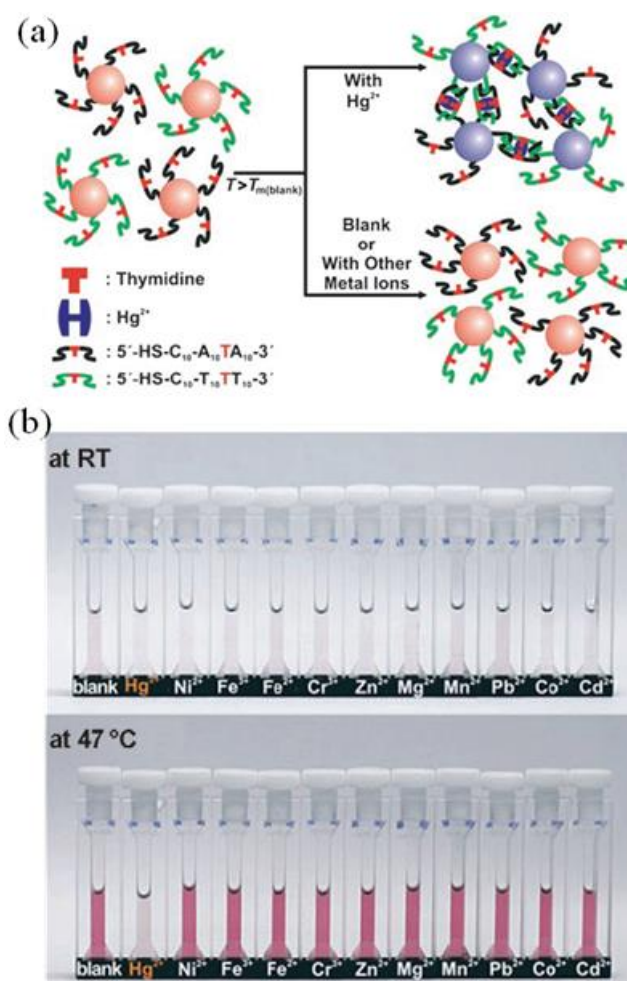


**Figure 5.** (a) Schematic illustration of the colorimetric detection of  $\text{Hg}^{2+}$  using DNA-Au nanoparticles, and (b) color change in the DNA-Au nanoparticle solution in the presence of various representative metal ions (each at  $1 \mu\text{M}$ ) upon heating from room temperature (RT) to  $47^\circ\text{C}$ . (Reprinted with permission from ref. 75, Copyright 2007, Wiley-VCH)

Further, Hupp *et al.*<sup>73</sup> extended the colorimetric technique to detect heavy metal ions such as  $\text{Pb}^{2+}$ ,  $\text{Cd}^{2+}$  and  $\text{Hg}^{2+}$  using 11-

mercaptoundecanoic acid (MUA) as a modifier for the Au nanoparticle surface. This modifier can recognize divalent metal ions by an ion-templated chelation process, wherein the binding of a divalent metal ion with a carboxylic group causes aggregation and a change in the extinction spectrum of the Au colloidal suspension. This technique has been further improved in sensitivity and specificity using DNA as the recognition element,<sup>74-76</sup> wherein the addition of metal ions results in the reversible association/dissociation of two complementary DNA-functionalized Au nanoparticles with intentionally designed base mismatches, forming DNA-linked aggregates, which change the color of the solution from red to blue.

Colorimetric detection of Hg<sup>2+</sup> using DNA-functionalized Au nanoparticles is demonstrated in Figure 5. When Hg<sup>2+</sup> is present in the solution, it selectively coordinates to the mismatched T-T base pair and allows quantification of the Hg<sup>2+</sup> concentration.<sup>75</sup> Liu *et al.*<sup>77</sup> simplified the DNA-Au nanoparticle based sensing system using an optimal DNA sequence to realize colorimetric detection of Hg<sup>2+</sup> at room temperature. This method has been extended to detect other metal ions by substituting the thymidine with synthetic artificial bases that selectively bind to other metal ions.<sup>78,79</sup> The LSPR of nanoparticles is highly dependent on the shape and size of the nanoparticle, with nanorods and nanoshells being more sensitive to changes in the local refractive index than solid nanospheres.<sup>80,81</sup> It has been reported that a nanorod's longitudinal LSPR mode exhibits six times higher sensitivity than a nanosphere counterpart.<sup>80</sup> The dependence of refractive index sensitivity on nanostructure's geometry can be understood conceptually by imagining how the concentrated charge and resulting EM field are screened by the refractive index. The sharper the tip or more "pointy" the nanostructure is, the more localized the EM field will be, and the more sensitive the concentrated electron density will be to shifts in the refractive index.

Nanoparticle-based colorimetric sensors are typically operated in a vial, requiring professionals in a laboratory. Real-world samples also need to be pre-treated in a laboratory prior to testing. To solve these problems, nanoparticle-based colorimetric sensors have been incorporated into lateral-flow strips to make a point-of-care device. For example, this type of device has been used to detect cocaine in serum,<sup>82</sup> proteins<sup>83</sup> and nucleic acids.<sup>84</sup>

The sensitivity of LSPR to the distance between coupled nanoparticles has also been used to develop a plasmonic molecular ruler (PMR).<sup>85,86</sup> PMRs can be used to measure the size of biomolecules in a label-free manner and to measure real-time molecular conformation changes and binding events. As compared to molecular rulers based on Förster resonance energy transfer (FRET), metal nanoparticle-based PMRs do not have photo-bleaching or blinking problems. In addition, PMRs are able to continuously monitor separations of up to 70 nm<sup>86</sup> as compared to the effective detection range of <10 nm for FRET.

An additional type of plasmonic nanoparticle-based sensor can be built according to the principles of plasmonic resonance energy transfer (PRET),<sup>87-90</sup> in which a plasmonic metal

nanoparticle serves as both the energy donor and the sensing reporter. When a plasmonic metal nanoparticle is in proximity to a molecule which has an absorption band overlapped with the LSPR, resonance energy transfer occurs between the metal and the molecule, giving rise to resonant quenching dips in the Rayleigh scattering spectrum of the metal particle. PRET sensors are suitable for both target detection and biomolecular imaging with nanoscale spatial resolution. Although the PRET method is superior in terms of sensitivity, selectivity, and multiplexing ability compared with methods based on dielectric property-induced shifts, it requires advanced instrumentation and algorithms to extract the molecule-plasmon interaction information.<sup>87-89</sup>

While plasmonic colloidal nanoparticle-based sensors provide a facile and rapid way to detect molecular or ionic targets using just the naked eye, this ease of use comes with the trade-off that their sensitivity (> nM in LOD) is lower compared with other optical or electrochemical techniques that can reach to pM or lower LOD in fluorescence, SERS, and electrochemical sensors. In addition, colorimetric detection typically suffers from interference problems when used in complex matrices; and their stability in a physiological solution is of concern because aggregation can occur in the absence of an analyte.<sup>91,37</sup> Efforts are therefore being made to develop robust colorimetric detection platforms for sensitive detection of analytes in real-world samples.

#### 4. Plasmon-enhanced fluorescence (PEF) sensors

The first PEF sensor was reported in 1991.<sup>92</sup> PEF is also referred to as surface plasmon-enhanced fluorescence spectroscopy (SPFS),<sup>93</sup> surface-enhanced fluorescence spectroscopy (SEFS), or metal-enhanced fluorescence (MEF). So far a standard naming convention for this type of sensor does not exist. PEF research was not active before 2007, but since this time, many nanostructures have been tested to plasmonically enhance fluorescence, coincident with the rise of controllable nanoparticle synthesis and lithography-based fabrication of nanostructured chips. The plasmon-induced fluorescence enhancement factor generally falls in the range of 10-100 but can be higher in optimized plasmonic nanostructures, even reaching to 1,340.<sup>94</sup> The rapid development of PEF sensors in the future is easily imaginable given the recent trends in nanofabrication and advancements in the understanding/theory of PEF. In contrast to previous review papers on PEF,<sup>95-97</sup> this review places an emphasis on the construction of PEF sensors and the underlying PEF principles.

##### 4.1 Mechanisms of plasmon-fluorescence interactions

The excited state of the fluorophore and plasmon must be understood before the plasmon-enhanced fluorescence mechanism can be described.<sup>28,30</sup> As shown in the Introduction, the energy of the plasmon is initially stored in the intense local EM field after excitation (Figure 1c). If the metal nanoparticle is small and electron scattering dominates, this energy is eventually converted into heat and the plasmon absorbs the incident light (Figure 1h). If radiative dampening dominates the

plasmon's decay, the energy is re-radiated into the far field as scatter (Figure 1i). The excited state of the fluorophore can be described by a similar radiative dipole model and will undergo the same excitation, relaxation, and absorption or re-radiation process when it interacts with light. However, there are several key differences. The fluorophore has a long-lived excited state on the order of nanoseconds that radiates strongly after thermal relaxation (the Stoke's shift) instead of the almost instantaneous scattering of the plasmon. As well, the absorption cross-section and local field of the few electron fluorophore are not as strong as the coherent, multiple electron plasmonic dipole.

The energy transfer between the plasmon and the fluorophore is dominated by dipole-dipole interactions, with the exact mechanism being determined by the separation distance. First, if the plasmon and the fluorophore are within ~1-10 nm of each other, the non-radiative local field of one dipole can excite the second one (Figure 6). This is known as Förster resonance energy transfer (FRET). The efficiency of energy transfer in FRET depends on two factors<sup>98</sup>

$$Eff_{FRET} = \frac{1}{1 + \left(\frac{R}{R_0}\right)^6} \quad (7)$$

The most obvious being the separation distance,  $R$ , which decays as  $1/R^6$  because each dipole has a  $1/R^3$  near field. The distance behavior is scaled by the factor  $R_0$ , which depends on the spectral overlap between the emission of the donor's excited state and the acceptor's ground state absorption. The value of  $R_0$  is usually in the range of 3-8 nm in plasmon/fluorophore FRET. The FRET process is very efficient, approaching 100% for  $R < R_0$  in the presence of plasmon, because of the amplified local field and large absorption cross-section inherent to LSPR. FRET can occur from plasmon to fluorophore or from fluorophore to plasmon.

Secondly, the plasmon can enhance the radiative rate of the fluorophore through the Purcell effect (Figure 6).<sup>99</sup> The Purcell effect can be understood as follows. If a radiative dipole is placed in a resonant cavity, the emission intensity will be amplified on-resonance and quenched off-resonance when compared to free space. This is because the cavity modifies the local density of optical states (LDOS) as follows<sup>99</sup>

$$\rho_{LDOS}(\omega) \sim |E_{loc}(\omega)|^2 \quad (8)$$

where  $|E_{loc}(\omega)|^2$  is the local electric field of the cavity normalized to the incident intensity. In air, the LDOS is constant and the dipole radiates equally at all emission energies. In the cavity, the LDOS is peaked at the resonance wavelength, and the dipole can emit into this mode at a higher rate than in air alone, like coupling into an antenna. The cavity can then re-radiate the transferred energy, resulting in an overall enhancement of the dipole's emission.

The plasmon has a local field  $|E_{loc}|^2$  stronger than the free space light incident on the nanoparticle, so it increases the LDOS compared to vacuum and acts like a resonant cavity for the fluorophore. If the plasmon's absorption or scattering

spectrally overlaps with the fluorophore's emission, the fluorophore's emission rate will be enhanced by the plasmon due to the change in the LDOS. The plasmon can either absorb the transferred energy or re-radiate it as scatter, resulting in a quenching or enhancement of the fluorophore's emission intensity. For a plasmonic dipole, the LDOS goes roughly as  $1/R^3$ , so the Purcell effect is usually seen outside the ~10 nm range of FRET where coupling goes as  $1/R^6$ .<sup>100-102</sup> It is possible that the plasmon's radiation or scattering rate can be enhanced by the fluorophore's LDOS. However, since the  $|E_{loc}|^2$  of the few electrons' oscillator dipole is usually on the order of free space, the resulting Purcell effect is negligible.<sup>101</sup>

The spectral overlap between the plasmon and the fluorophore determines whether FRET or the Purcell effect is present and whether these mechanisms lead to an enhancement or quenching of the fluorophore emission (Figure 6). If the plasmon overlaps with the fluorophore's absorption, the excitation rate of the fluorophore will be enhanced from its free space value (Figure 6a).<sup>28,30,100-105</sup> For metal nanoparticles which primarily absorb, usually smaller than ~15 nm, the fluorophore will be excited through FRET by the intense local field of the plasmon. For larger metal nanoparticles which primarily scatter, usually greater than ~15 nm, an enhancement will be possible through both FRET at close distances (~10 nm) and the Purcell effect at longer distances (~10-50 nm) (Figure 6c).<sup>28,30,100-105</sup> As mentioned, the Purcell enhancement for the plasmon's radiation is usually negligible because the LDOS for the fluorophore is negligible, meaning that the excitation enhancement is primarily dominated by FRET at distances of a few nanometers.<sup>101</sup> The excitation enhancement is maximized by using nanoparticles which absorb and do not scatter light, plus concentrate the local field in gaps or sharp points (Figure 6d). Given the trade off between FRET and the Purcell effect, changes in distance of a few nanometers will greatly change the excitation enhancement, allowing a sensor to be built which is highly responsive to minimal changes in the local environment.

If the plasmon is overlapped with the fluorophore's emission, an enhancement or quenching of the emission intensity is possible (Figure 6b).<sup>28,30,95,100-105</sup> If the fluorophore is within a few nanometers of the plasmon, its emission will be quenched by FRET into the plasmon. Although the plasmon could re-radiate this energy enhancing the emission intensity, the near field of the dipole also excites higher order modes in the plasmon which cannot re-radiate into the far field, leading to an overall quenching at separation distances of a few nanometers (Figure 6c). At distances beyond FRET, a strong Purcell enhancement will be induced because of the enhanced LDOS of the plasmonic field relative to free space. This will lead to an increase of the radiative rate of the fluorophore compared to free space, and if the plasmon can scatter more efficiently than it absorbs, will result in an fluorescence emission enhancement. Metal nanoparticles with higher scattering than absorption efficiencies and separation distances beyond where non-radiative transfer is efficient will maximize the emission enhancement (Figure 6d). It is usually very difficult, however, to obtain a pure excitation or emission

enhancement because of the limited Stoke's shift of the dye and large absorption and scattering line widths of the plasmon relative to the fluorophore. Instead a balance is present between each effect. Generally this leads to a strong quenching being present at a few nanometers distance, which transitions into a large enhancement of 10-100 times in the range of ~10-30 nm, and then slowly returns to normal emission strengths as the separation distance approaches hundreds of nanometers (Figure 6d).<sup>106-115</sup>

When designing a sensor, the PEF theory can be simplified to manageably guide fabrication choices by considering three factors including (i) the enhancement of EM field induced by the plasmon, (ii) the spectral overlap of the plasmon's absorption and scattering with the absorption and emission band of fluorophore and (iii) the gap (or space) between the

plasmonic metal and the fluorophore. First, the total enhancement in excitation or emission can be thought of as  $|\vec{E}_{dipole}|^4 / |\vec{E}_{higher\ order}|^2 \sim |\vec{E}|^2$  for most plasmonic structures.<sup>116</sup> The quantity  $|\vec{E}|^2$  can be easily estimated by FDTD simulations, helping to predict the enhancement in more complex structures.<sup>19,117</sup> Second, the optimal positioning of the spectral overlaps will be defined by the separation distances possible and the size of the metal nanostructure (whether it absorbs or scatters). If metal nanoparticles which primarily absorb (less than ~15 nm) can be used over distances less than ~10 nm, the plasmon should be overlapped with the excitation of the fluorophore to avoid emission quenching. If nanoparticles which primarily scatter can be used, and precise control over distance is possible, the plasmon should

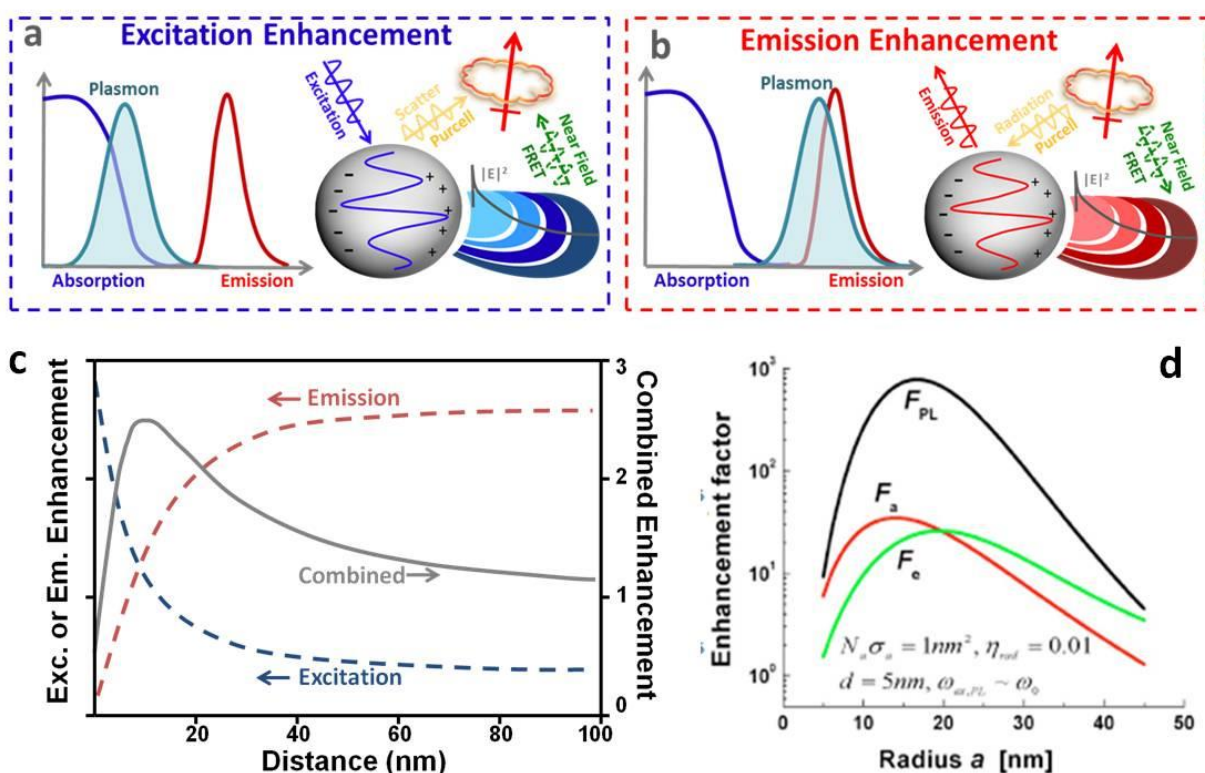


**Figure 6.** Dependence on distance and sphere radius of plasmon-enhanced fluorescence. (a) If the plasmon overlaps with the absorption of the fluorophore, an excitation enhancement is possible through the near field and FRET or scattering. (b) If the plasmon overlaps with the emission of the fluorophore, an emission enhancement is possible through the Purcell effect or FRET. (c) The excitation enhancement (red line) falls off quickly with distance, while the emission enhancement (blue line) is quenched at short distances but increases rapidly. The combined photoluminescence enhancement, equal to the emission enhancement times the excitation enhancement, peaks at around 10-30 nm. (Adapted from ref. 111). (e) The optimal sphere radius for excitation (red line), emission (green line), and total photoluminescence enhancement (black line) varies with the balance between absorption and scattering. (Reprinted with permission from ref. 101, Copyright 2009, Optical Society of America).

overlap both peaks with a separation of around ~10-30 nm to achieve the maximum fluorescence enhancement (Figure 6d).<sup>28,30,95,100-105,110-112</sup> The balance of quenching and fluorescence, while difficult from an optimization standpoint, allows sensors to be constructed that heavily modulate the fluorescence intensity through the interaction with a single analyte.

Finally, it should be noted that the plasmon can also absorb or scatter the fluorophore's emission in the far field beyond the

range of PEF, distorting the measured spectrum. The far field scattering of the plasmon can also increase the path length of light in the solution or matrix holding the fluorophore, increasing the measured absorption efficiency. The far field interactions are not useful for sensors since they do not have a dependence on inter-nanoparticle distance allowing modulation, however, they can be useful as a passive component of a pre-existing fluorescence sensor to increase the measured signal. It

should also be noted that the quantum efficiency of the fluorophore is also important, as PEF cannot occur if the efficiency of the dye is already 100%.<sup>101</sup>

#### 4.2 Colloidal nanoparticle-based PEF sensors

For free-standing colloidal nanoparticles, a strong LSPR can be excited and SPP cannot exist. Hence, only LSPR can be used to enhance the fluorescence of colloidal nanoparticle-based sensors *via* the excitation and/or emission enhancement.<sup>118-127</sup> In the case of the excitation enhancement, the LSPR peak should be close to the absorption band of the fluorophore<sup>128</sup> and the separation between the fluorophore and the plasmonic nanoparticle should be minimized (Figure 6c). In the case of the emission enhancement, the LSPR peak position should be closer to the emission peak of the fluorophore<sup>111,113</sup> and the separation between the fluorophore and the plasmonic nanoparticle should be controlled to 10-30 nm. For the emission enhancement, the larger the plasmonic nanoparticle is, the stronger the fluorescence enhancement will be due to the increased scattering effects.<sup>129</sup> In both cases, stronger local EM fields will lead to higher enhancements. Hence nanostars, nanorods, and nanoshells generally have an increased PEF effect compared to nanospheres.<sup>130</sup>

Hu *et al* developed a plasmon-enhanced fluorescence probe based on these principles (Figure 7a).<sup>131</sup> First, an anti-apptamer linked with a Cyanine 3 dye is coupled to a prion protein. Second, the Ag@SiO<sub>2</sub> core-shell nanoparticles are conjugated with an aptamer, allowing capture of the prion protein. This means that the fluorescence emission is enhanced by the LSPR of the Ag nanoparticles only when captured, producing a sensor. This PEF probe was used to successfully image the prion protein in living SK-N-SH cells (Figure 7b). In addition, Lu *et al* developed a Ag@SiO<sub>2</sub>@aptamer-Cyanine 5 nanoparticle for detection of adenosine-5'-triphosphate (ATP).<sup>132</sup> The aptamer linked with Cyanine 5 dye was immobilized on the nanoparticle surface *via* hybridization with the complementary DNA in the absence of ATP, showing a 32-fold enhancement compared to free-standing Cyanine 5 in solution. When ATP was present in solution, the binding of the aptamer with the DNA led to detachment of the aptamer-Cyanine 5 from the nanoparticle surface, modulating the fluorescence. This PEF sensor exhibited a linear response from 0 to 0.5 mM and a limit of detection (LOD) of 8  $\mu$ M toward ATP.

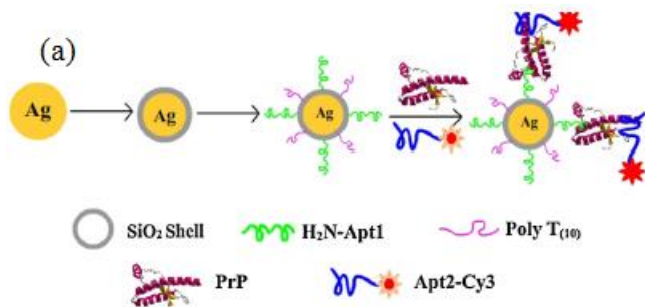


**Figure 7.** (a) Schematic illustration of plasmon-enhanced fluorescence detection of prion proteins; (b) distribution of the Ag@SiO<sub>2</sub>-Cyanine-labeled prion protein after endocytosis in living SK-N-SH cells. (Reprinted with permission from ref. 132, Copyright 2013, Elsevier).

#### 4.3 Chip-based PEF sensors

As compared to colloidal nanoparticle-based sensors, chip-based sensors provide better reproducibility and a larger area/volume of “hot spots” allowing higher sensitivity to be achieved.<sup>133</sup> The fluorescence can be enhanced *via* the different excitation and emission enhancements possible on different plasmonic substrate configurations. For example, the ELISA-analogous sandwich configuration is commonly used in immuno-assays. For conventional chip-based sandwich immuno-sensors, the capture antibody is immobilized on a solid substrate, the antigen (analyte) is sandwiched between the capture antibody and the detection antibody that is linked to a fluorescent dye. To improve the sensitivity of this configuration, a plasmonic nanoparticle can be conjugated to the fluorescent dye molecule to amplify the fluorescence signal *via* LSPR.<sup>134-136</sup> Chang *et al* used this strategy to develop a PEF biosensor for the detection of the pancreatic cancer marker ULBP2. The LOD of the biosensor was improved by 100-fold and reached 16–18 pg/mL in 1% BSA–PBS and in 10-fold-diluted human serum.<sup>134</sup>

Fluorescence can also be enhanced *via* excitation of the LSPR of randomly distributed metal nanoparticles (such as a Ag island film) or a periodic nano-array pattern on a solid substrate.<sup>137-139</sup> Recently, Xie *et al* utilized a Ag nano-triangle array to enhance the fluorescence of near-infrared (NIR) dyes.<sup>140</sup> NIR dyes in the “water window” (700-900 nm) are of particular interest to bio-sensing and bio-imaging since this spectral window allows deep penetration into biological fluids, cells, and tissues. As well, at these wavelengths, the auto-fluorescence of biomolecules is minimal, reducing interference. Xie’s results have shown that the fluorescence of a low quantum-yield (4%) NIR dye (Alexa Fluor 790) can be enhanced by two orders of magnitude using the Ag triangle array pattern. The SPP in a nano-hole array pattern allows for extraordinary optical transmission, which has been used to enhance the fluorescence of a dye by two orders of magnitude compared to a reference counterpart on a glass support.<sup>141</sup>

As mentioned, SPP-based sensors were initially engineered using a metal film on a prism. The SPP field decays exponentially with a length of hundreds of nanometers,<sup>13</sup> leading to a fluorescence excitation enhancement over a longer distance than LSPR.<sup>28,30,95</sup> The SPP cannot re-radiate the absorbed energy into free space due to the momentum mismatch, so when a fluorophore is coupled into the SPP, the SPP re-radiates the fluorescence into the coupling prism or grating, leading to an angle-resolved emission (Figure 1g).<sup>13,28,30,95</sup> This well-known phenomenon is referred to as surface plasmon-coupled emission and occurs when the excited fluorophores are positioned up to 200 nm from a continuous thin metallic film (~20-50 nm thick).<sup>96,142</sup> If the fluorophore is at distances of a few nanometers to the metal film, the fluorophore can induce charge oscillations in the metal film, leading to quenching through FRET or coupling to lossy surface waves. Energy cannot be coupled into the SPP in this manner so no re-radiation through the coupling prism or grating exists, only quenching of the fluorescence. SPP-enhanced fluorescence offers the ability to selectively detect analytes with many advantages such as high spatial resolution, suppressed background interference, *p*-polarized emission, and a large effective detection distance. SPP-enhanced fluorescence has been used for detection of nucleic acids, proteins and other chemicals.<sup>143-145</sup> LRSP-based PEF sensors with a penetration depth on the micron scale are of particular interest in the analysis of large analytes such as bacteria and tissues.<sup>146-148</sup> For example, Huang *et al* developed a LRSP-based PEF sandwich immunoassay that was able to detect *E. coli* O157:H7 with a LOD of 6 colony forming units (CFU/mL).<sup>147</sup> In addition, a LRSP-based PEF sensor exhibited a LOD of 34 fM and 330 fM toward a prostate specific antigen (PSA) in a buffer and in human serum, respectively.<sup>149</sup> It is worth noting that the LOD of the LRSP-based PEF sensor was four orders of magnitude better than detection using the plasmon peak shift with refractive index.

#### 4.4 Plasmon-enhanced FRET sensors

FRET is a very efficient method for transferring energy between two dipoles at a distance of a few nanometers and allows for minimal analyte changes to translate into modulation of the signal.<sup>150-161</sup> The incorporation of plasmons into FRET offers even greater flexibility for modulating the energy transfer process because of the plasmon's large absorption and scattering cross-section compared to its size as well as the strong local EM field compared to incident light.<sup>162-164</sup> The plasmon can play two unique roles in FRET: (i) acting as the energy acceptor that quenches the fluorophore, and (ii) serving as the third party that modulates the energy transfer between the donor and the acceptor.<sup>165-169</sup>

When the plasmon acts only as the energy acceptor, it is ideal to use nanoparticles with high absorption cross-sections and intense local fields but little scattering. This ensures that the plasmon only quenches the fluorescence and does not enhance the fluorescence intensity.<sup>28,30,100-105</sup> Plasmonics offers two key advantages over organic dyes as an acceptor. First is

the larger absorption cross-section which allows higher quenching efficiencies. The higher quenching efficiency leads to sensing distances up to twice that found in a fluorophore-fluorophore FRET system.<sup>170,171</sup> Second, when designed properly, the plasmon does not re-radiate energy, reducing the background signal levels. These advantages are demonstrated in a recent study on the CdSe/ZnS quantum dot (QD)-Au system which showed that the energy transfer efficiency and mechanism depend on the size of the Au nanoparticles (Figure 8).<sup>163</sup> For 3 nm Au nanoparticles where LSPR is absent due to quantum size effects, energy transfer proceeds through nano-surface energy transfer (NSET) rather than FRET. In NSET, the energy is transferred into individual electron-hole pairs instead of the collective LSPR mode, leading to a quenching rate of  $1/R^4$ .<sup>163,172</sup> According to the NSET mechanism, a QD-DNA-Au ensemble was designed to detect Hg(II) ions.<sup>173</sup> This nanosensor exhibited a LOD of 1.2 ppb toward Hg(II) in the river water, which was lower than the maximum allowable levels of Hg(II) in drinking water (2 ppb) regulated by the U.S. Environmental Protection Agency (EPA).

Biological molecules can modulate and switch on/off the energy transfer process in FRET. This strategy has been extensively used to study intermolecular interactions, quantify analytes, and *in vivo* generate biological images.<sup>174,175</sup> Plasmonic nanoparticles (*i.e.* Au and Ag) have many advantages as the energy acceptor in FRET sensors,<sup>163,176,177</sup> including (i) high fluorescence quenching efficiency compared to organic dyes because of the stronger LSPR absorption (molar extinction coefficients up to  $10^{10}$  cm<sup>-1</sup>·M<sup>-1</sup>), (ii) tunable quenching, (iii) limited photo-stability problems, and (iv) ease of labeling for biocompatible applications. Therefore,

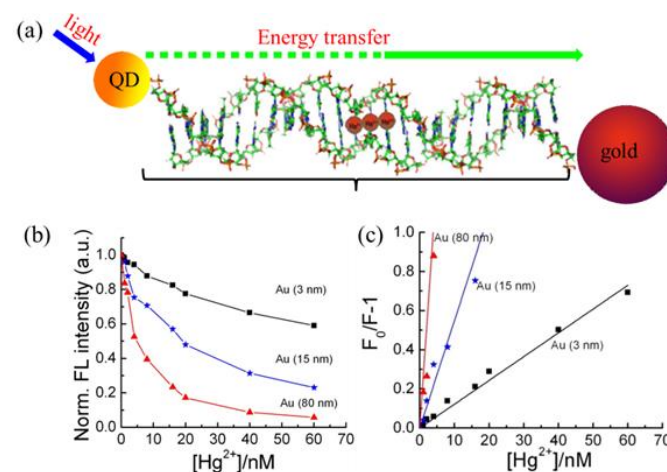


**Figure 8.** (a) Schematic illustration of CdSe/ZnS quantum dot-Au nanoparticle energy transfer. The CdSe/ZnS quantum dots with fluorescence emission at 572 nm were used as the energy donor while different sized Au nanoparticles (3, 15 and 80 nm) were used as the energy acceptor. Two complementary single stranded DNA strands with deliberately designed T-T base mismatches are employed to control the separation distance. (b) Normalized fluorescence emission intensity at 572 nm as a function of the Hg<sup>2+</sup> ion concentration. (c) Stern-Volmer plots showing the quenching efficiencies by the Au nanoparticles. (Reprinted with permission from ref. 163, Copyright 2011, American Chemical Society).

incorporation of plasmonic nanoparticles into energy transfer-based fluorescence sensors has led to great success in improving the sensitivity, stability, and reproducibility of FRET based sensors.

Another route is plasmon-mediated FRET in which a plasmonic nanostructure is used as a mediator rather than a donor or an acceptor. The plasmon can lead to both excitation and emission enhancements for both the donor and the acceptor. For PEF, these two effects are balanced *vs* the distance for each fluorophore. The distance must be balanced to either individually increase the excitation and emission of the donor and acceptor, or collectively mediate the emission of the donor into the acceptor.<sup>168,178-181</sup> For plasmon-mediated FRET, the donor's emission spectrum and the acceptor's absorption are required to overlap with the plasmon absorption. The energy is first absorbed by the donor and then transferred to the plasmon. If at close distance of a few nanometers, this transfer will occur by FRET and through the Purcell effect to higher order modes, which mainly leads to quenching but can also lead to re-radiation of the plasmon into the acceptor.<sup>28,30,100-105</sup> If outside the FRET range, the donor can radiate into the plasmon by the Purcell effect, similar to the emission enhancement.<sup>168,178,181</sup> The plasmon can then re-radiate this energy to the acceptor by FRET or the Purcell effect, just like PEF with a plane wave incident field, leading to an excitation enhancement for the donor.<sup>28,30,100-105</sup> Unfortunately, the small Stoke's shift of most quantum dots and dyes means that the donor's emission and absorption strongly overlap, as does the acceptor's emission and absorption, preventing the ideal chain of energy transfer. Instead the combined excitation and emission enhancements of the donor and acceptor must be taken into account as well as the plasmon mediated field.

A plasmon-mediated FRET sensor has been developed for detection of human platelet-derived growth factor-BB (PDGF-BB).<sup>182</sup> A fluorophore-linked single-stranded DNA and a quencher-terminated complementary DNA formed a DNA duplex with both the fluorophore and the quencher at the same end, enabling the FRET process. This FRET sensor was immobilized on the surface of a Ag nanoparticle so that when PDGF-BB bound to the DNA strand was functionalized with the quencher, the DNA duplex was disrupted, leading to the detachment of the quencher from the fluorophore. FRET is then disabled and the fluorophore re-emits, modulating the signal. The sensor had a linear range of 6.2-50 ng/mL with a LOD of 0.8 ng/mL. When the Ag nanoparticle was not used, replaced with a Au nanoparticle, or substituted with a shifted, non-matching LSPR peak, the sensitivity of the sensor was reduced, proving that the spectral position of the LSPR played a key role in determining if the energy transfer was possible. Zhou *et al* recently reported a fascinating plasmon-mediated energy transfer sensor for Hg(II) detection.<sup>183</sup> A 6-carboxyfluorescein (FAM) dye and a Ag nanoparticle were linked to two opposite ends of an aptamer to form a hairpin-shaped molecular beacon. Initially, the fluorescence emission of the FAM dye was quenched due to its proximity to the plasmonic Ag nanoparticle. When Hg(II) ions were added, the aptamer

stretched due to DNA hybridization, leading to the formation of a gap larger than the FRET distance between the FAM dye and the Ag nanoparticle. The large gap relative to the FRET distance means that the LSPR of the Ag nanoparticles only enhanced but not quenched the fluorescence of the FAM dye when Hg(II) ions were present, signalling the presence of the ions. This sensor achieved a LOD of 1 nM toward Hg(II) in a phosphate saline buffer.

## 5. Surface-enhanced Raman scattering sensors

### 5.1 SERS enhancement mechanisms

SERS continues to attract increasing attention as an analytical technique for chemical sensing and biomedical applications due to several advantages,<sup>184-186</sup> including (i) the unique spectral signatures of analytes, (ii) no interference from water, (iii) easy operation without complicated sample preparation, (iv) multiplexing detection capability with a single excitation laser due to the narrow bandwidth spectral features, (v) high-throughput and point-of-care applications from commercially available portable Raman spectrometers, and (vi) single-molecule sensitivity.<sup>187-195</sup> Both electromagnetic (EM) enhancement and chemical enhancement (CE) contribute to the overall SERS enhancement. The EM enhancement originates from the amplified local EM field in plasmonic nanostructures while the CE mechanism is due to charge transfer between the metallic nanostructures and the adsorbed molecules.<sup>25,186,195</sup> The EM enhancement is typically the largest contributor to SERS, yielding enhancements anywhere between  $10^4$  and  $10^8$ , while the CE process yields an enhancement factor of 10 to 100.<sup>25,196-199</sup> The EM field enhancement can be understood as the limiting case of PEF, where the small Raman scattering cross-

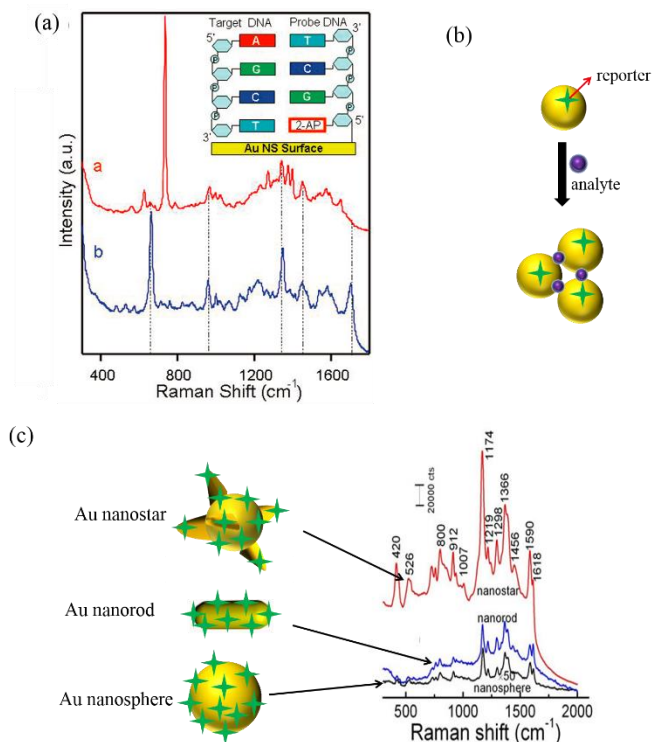


**Figure 9.** (a) Assay of DNA hybridization using SERS via direct readout of spectral signatures of DNA bases. (Reprinted with permission from ref. 204, Copyright 2013, American Chemical Society). (b) Analyte-induced SERS enhancement through aggregation of plasmonic nanoparticles where Raman reporters are directly adsorbed on the particle surface. (c) Shape-dependent SERS enhancement. (Reprinted with permission from ref. 19, Copyright 2005, IOP Publishing.)

section cannot induce quenching in the plasmon, making  $|\vec{E}_{higher\ order}|^2$  negligible and leading to a  $|\vec{E}_{loc}|^2$  enhancement during both excitation and emission. The difference in excitation and scattered Raman frequency is usually taken as negligible, leading to an overall enhancement of  $|\vec{E}_{dipole}|^4 / |\vec{E}_{higher\ order}|^2 \cong |\vec{E}_{loc}|^4$ .<sup>116,200</sup> Since the local field of the plasmon can be several orders of magnitude higher than that of the incident field, SERS signals can be detected even though the Raman scattering cross-section is itself very small ( $\sim 10^{-30}$  cm<sup>2</sup>/molecule), leading to the EM enhancement mechanism being preferred in most SERS-based sensors. The design and fabrication of plasmonic nanostructures is the key for high-performance SERS sensors since the maximum field enhancement determines the sensitivity, reproducibility and applicability of the sensor.

## 5.2 Colloidal nanoparticle-based SERS sensors

One of the unique features of SERS sensors is that an analyte can be identified by its unique Raman spectrum, providing a route for label-free detection. Unfortunately, Raman scattering itself is inefficient because of the small scattering cross section ( $10^{-28}$ – $\sim 10^{-30}$  cm<sup>2</sup>/molecule), which is 12–14 orders of magnitude lower than the absorption cross section of fluorescent dyes.<sup>201</sup> The Raman signal is therefore difficult to use in a sensor, as it is very weak for a low concentration of

analyte. The analyte's low scattering cross section can be overcome, however, by designing plasmonic structures to either enhance the intrinsic SERS signal of the analyte, or using an extrinsic design where the SERS signal of a reporter molecule is only enhanced in the presence of the analyte.

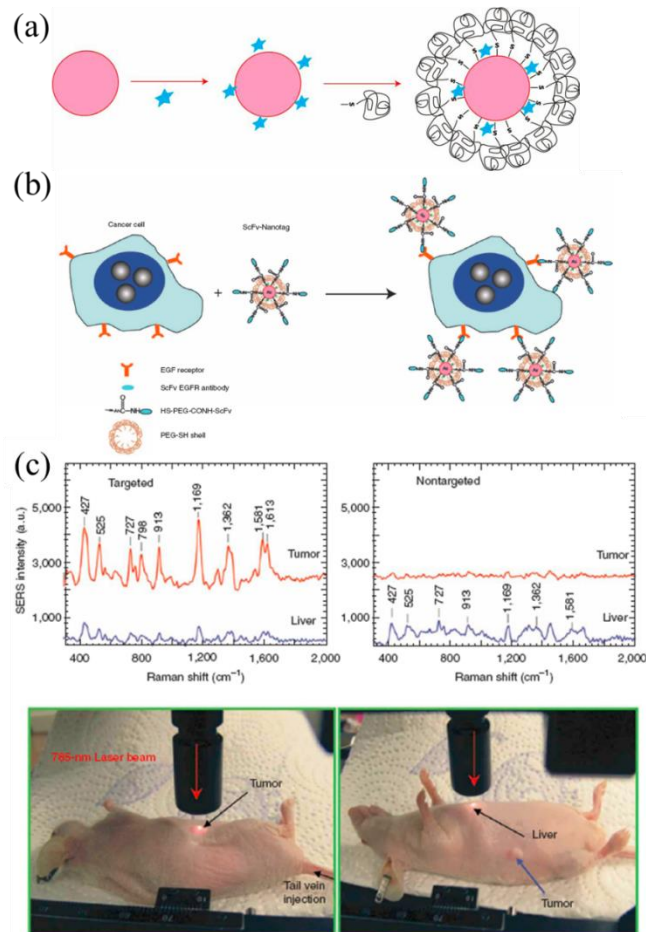


**Figure 10.** (a) Preparation and schematic structures of Au nanoparticles encoded with a Raman reporter and coated with a layer of thiol-PEG. (b) Preparation of targeted SERS tags by using a mixture of thiol-PEG and a heterofunctional PEG. Covalent conjugation of an EGFR-antibody fragment occurs at the exposed terminal of the heterofunctional PEG. (c) *in vivo* cancer targeting and SERS detection by using ScFv-antibody conjugated Au nanoparticles that recognize the tumor biomarker EGFR. SERS spectra were obtained from targeted and nontargeted SERS tags. Photographs showed a laser beam focusing on the tumor site or on the anatomical location of liver. (Reprinted with permission from ref. 234, Copyright 2007, Nature Publishing Group).

For example, DNA bases can be identified by their intrinsic SERS spectral signature after directly binding onto a Au nanoshell nanoparticle (Figure 9a).<sup>202–205</sup> The extrinsic method is popular as it allows detection of analytes with weak or non-existent SERS signals. One method for achieving a strong SERS signal in the absence of an intrinsic signal is to conjugate Raman reporter molecules onto a plasmonic colloidal metal nanoparticle, forming a SERS label (tag) similar to a fluorescent dye tag. Nitrogen- and sulfur-containing molecules are usually used as Raman reporters because of their large affinity to typical plasmonic metals such as Au and Ag. The

plasmonic field of the nanoparticle increases the SERS signal of abundant Raman reporter molecules, increasing the minimum detectable concentration compared to the intrinsic signal of a single molecule. Additionally, once an analyte is present, the distance between nanoparticles can be reduced and the plasmonic field increased (Figure 9b), multiplying the SERS signal of abundant Raman reporter molecules covering the surface of the nanoparticle. This results in an amplified signal. Even only one analyte molecule may cause the aggregation of nanoparticles, the signals of abundant Raman reporter molecules are enhanced. The amplification effect is maximal when the excitation wavelength of the laser source is overlapped with the LSPR of the nanoparticle,<sup>19</sup> a condition referred to as resonance enhancement.

Maximizing the plasmonic EM field is critical to the development of a sensitive SERS probe. Many efforts have therefore been devoted to tailoring the SERS substrate.<sup>206-217</sup> A recent study has investigated the effect of the Au nanoparticle shape on the SERS enhancement.<sup>19</sup> The results have showed that nanorods have a larger enhancement than nanospheres (Figure 9c), and Au nanostars exhibited the strongest SERS enhancement, which is attributed to the highly concentrated EM field in the sharp tips, similar to a lightning rod. Recently, a colloidal gold nanostar-based SERS sensor was developed for detection of glucose in saliva using optimization of the SERS substrate.<sup>218</sup> In this sensor design, Au nanostars were conjugated with a glucose oxidase enzyme. When glucose was present, the enzyme molecules produced H<sub>2</sub>O<sub>2</sub>, which was detectable by SERS because of amplification by the Au nanostar's local EM field. In another approach, an interesting SERS substrate has been developed by an "On-Wire" lithography method. Multiple nano-gaps were fabricated in individual metal nanowires to form "hot spots", resulting in a stronger SERS enhancement.<sup>219,220</sup>

Poor reproducibility often exists when Raman reporter molecules are directly adsorbed onto a bare nanoparticle's surface as a SERS tag. One problem is that the SERS tags can aggregate in a high strength ionic solution to the point of becoming sediment. Also, the Raman reporter molecules can easily desorb from the nanoparticle surface, leading to a loss of signal during detection. To overcome these issues, the Raman reporter molecules can be encapsulated between a metal core and a thin protective layer (e.g., polyethylene glycol (PEG) or SiO<sub>2</sub>) to form a sandwich-structured SERS tag.<sup>19,221-229</sup> The sandwiched SERS tag offers several appealing features,<sup>19,226-228</sup> such as (i) encapsulating a large number of Raman reporter molecules in a single particle, leading to a strong SERS signal; (ii) preventing leaching out of the Raman reporter molecules; (iii) enabling excellent water-solubility due to high hydrophilicity of the shell surface; and (iv) providing further flexibility for bio-conjugation. SiO<sub>2</sub> is of particular interest as the shell material because current synthetic chemistry techniques are able to obtain a very thin SiO<sub>2</sub> layer (1-2 nm thick) on the surface of Au nanoparticles using sodium silicate as a precursor; and the SiO<sub>2</sub> layer is dense, biocompatible, water-soluble, and easy to surface-functionalize.<sup>19,224,225,229</sup> For

example, sandwich nanoparticles with a thin SiO<sub>2</sub> outer-layer have been used for selective imaging of a target protein in prostate tissue.<sup>229</sup>

Biocompatible and nontoxic sandwich SERS probes have been demonstrated in drug delivery and *in vivo* tumor detection. Delivery and release of drugs can be tracked by the SERS signals, which is advantageous since a near-infrared laser source can penetrate into biological fluids and thick tissues.<sup>230-233</sup> Nie and coworkers<sup>234</sup> have reported *in vivo* tumor targeting and spectroscopic detection using a sandwich SERS tag with a PEG shell (Figure 10). The pegylated sandwich SERS tag exhibited excellent *in vivo* bio-distribution and pharmacokinetic properties as well as good colloidal stability over a wide range of pH and ionic strength, and thus superior performance to near-infrared semiconductor quantum dots. When conjugated to tumor-targeting ligands, the conjugated SERS tags were able to target tumor biomarkers such as the epidermal growth factor receptors on human cancer cells and in xenograft tumor models.

### 5.3 Chip-based SERS sensors

Solid-state chip-based plasmonic substrates utilizing both LSPR and SPP have been extensively used in the construction of SERS sensors. For example, Au and Ag nanoparticles have been immobilized on a solid-state chip *via* a self-assembly method to serve as a SERS substrate.<sup>235</sup> In another design, a ~1 μm silver nanorod array layer was grown on a pre-deposited 500 nm silver film by oblique angle deposition.<sup>236</sup> SERS spectra were obtained for several whole cell bacteria that were sitting on the silver nanorod array, such as Generic *Escherichia coli*, *E. coli* O157:H7, *E. coli* DH 5α, *Staphylococcus aureus*, *S. epidermidis*, *Salmonella typhimurium*, and bacteria mixtures. Principal component analysis (PCA) was used to recognize the patterns of the SERS spectra and differentiate the Gram types, different species, and strains, demonstrating the feasibility of label-free SERS detection of bacterial pathogens.

An alternative way to make a SERS substrate is to generate nanostructures with the assistance of templates. For example, a Ag film can be deposited over a self-assembled polystyrene nanosphere monolayer on a solid-state support. This Ag film-on-nanosphere (AgFON) structure shows strong LSPR.<sup>237,238</sup> The AgFON has been used to identify *Bacillus subtilis* spores, which are the simulants for *Bacillus anthracis*,<sup>239</sup> achieving a LOD of  $2.6 \times 10^3$  spores. A large-area periodic nano-array pattern provides better reproducibility and controllability for SERS sensing than non-periodic metal nanoparticles. For example, Van Duyne and co-workers have fabricated plasmonic nano-triangle arrays using nanosphere lithography.<sup>240</sup> The LSPR peak of a Ag nano-dot array can be systematically tuned in a wide range (400 to 6000 nm) by tailoring the gap, size, and height of the nano-dots; and the sharp tips of the nano-triangle can achieve an EM enhancement factor of  $\sim 10^8$ .<sup>241,242</sup> Additionally, strong "hot spots" are generated in the small gap between triangles when the nano-triangles are brought in proximity to form a bowtie structure. A gold bowtie with a gap of  $8 \pm 1$  nm exhibited a SERS enhancement factor of  $10^{11}$ .<sup>243</sup> The SPP-induced "extraordinary optical transmission" effect in

a nano-hole array has also been utilized to enhance the SERS signal,<sup>244-245</sup> with the enhancement maximized when the excitation wavelength of the laser matched the largest transmission peak of the nano-hole array. It is worth noting that LRSP modes have also been utilized to generate angle-dependent SERS with a SERS enhancement factor of  $9.2 \times 10^8$ .<sup>246</sup>

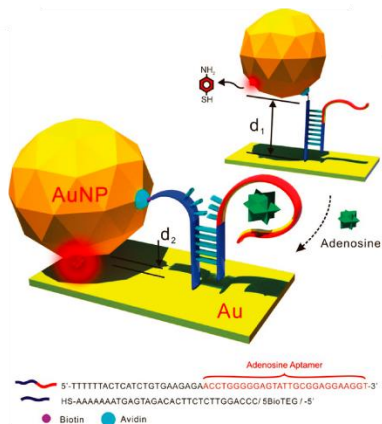


**Figure 11.** Scheme of SERS detection of adenosine through the plasmonic coupling of Raman reporter-labeled Au nanoparticles and a Au film. (Reprinted with permission from ref. 206, Copyright 2013, American Chemical Society).

It should be pointed out that the size, shape, and pitch of the nano-array define the effectiveness for SERS enhancement. For example, if a large SERS enhancement is to be formed using the strong “hot spots” that exist between the individual dots in a nano-dot array, the edge-to-edge gap must be less than 40 nm. Unfortunately, it is difficult to obtain patterns of this scale using conventional photolithography. Electron-beam lithography and focused ion beam lithography are able to produce nano-array patterns with these features, however both methods are low-throughput and cannot massively fabricate large-area nano-array patterns. More recent fabrication techniques promise to overcome this barrier, with nanosphere lithography and nanoimprinting lithography, offering a promising route to massively produce large-area periodic nano-array patterns at a relatively low cost.

As shown in Figure 11, coupling SERS labels (tags) onto a chip is an excellent method to construct SERS sensors, showing higher sensitivity and selectivity as well as better anti-interference capability.<sup>186, 187, 189, 206, 247-255</sup> As seen in Figure 12a, Au nanostar@Raman reporter@SiO<sub>2</sub> sandwich SERS tags were used for detection of adenosine triphosphate (ATP) by bringing the SERS tags in proximity to a gold chip.<sup>187</sup> In this SERS sensor, the aptamer labeled with the SERS tag was hybridized with complementary single-stranded DNA on the Au chip to form a rigid duplex DNA. When ATP was present, the binding of the aptamer with ATP led to the removal of the aptamer-linked SERS tag from the Au chip, modulating the SERS signal. This SERS sensor has achieved a LOD of 12.4 pM for ATP detection. The availability of substrates with high enhancement factors is the key to the success of SERS-based sensors. In the above-mentioned ATP sensor, the SERS

enhancement mainly came from the plasmonic field of the individual Au nanostars with the weak coupling between the Au nanostars and the Au chip. A different nano-architecture was therefore designed to couple the plasmonic fields and further enhance the EM field both in intensity and in space/volume.<sup>189</sup> Three different configurations of SERS immunoassays were constructed including (i) Au sphere@MGITC@SiO<sub>2</sub> SERS tags coupled to a planar Au film (where MGITC stands for malachite green isothiocyanate, a Raman reporter), (ii) Au sphere@MGITC@SiO<sub>2</sub> SERS tags coupled to a Au triangle nanoarray pattern, and (iii) Au star@MGITC@SiO<sub>2</sub> SERS tags coupled to a Au triangle

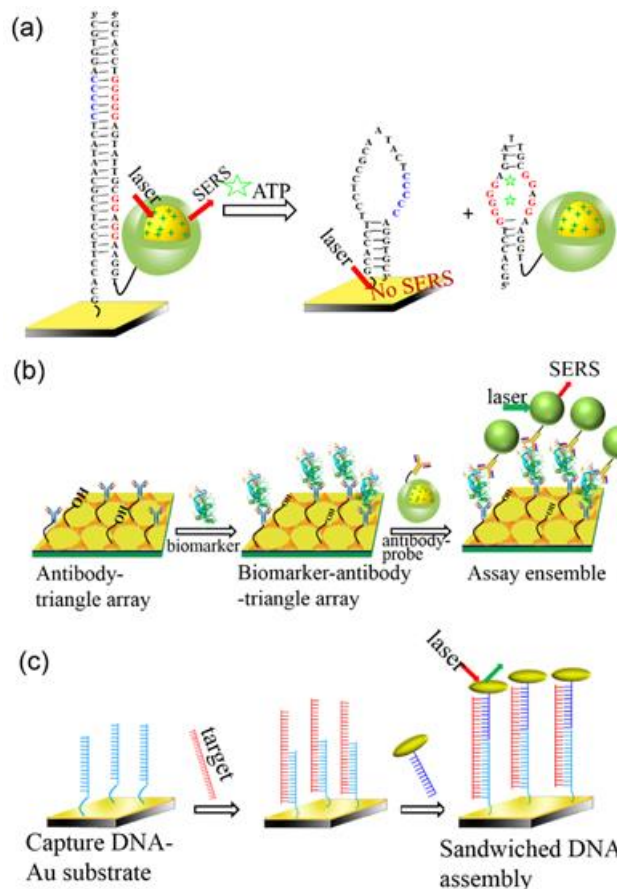


**Figure 12.** Schemes of sandwich SERS tag-based assays of (a) ATP, (b) cancer biomarkers in blood plasma, and (c) hepatitis B DNA (Reprinted with permission from refs. 186, 187 and 189, Copyrights 2012, 2013, American Chemical Society).

nanoarray. The Au star@MGITC@SiO<sub>2</sub>/Au triangle nanoarray showed the highest sensitivity due to the generation of a larger density of “hot spots” in the 3D plasmonic nano-architecture. The SERS signal exhibited a dynamic linear range of 0.1 pg/mL up to 10 ng/mL and a LOD of 7 fg/mL toward immunoglobulin G (IgG) protein in a buffer solution. The biosensor also demonstrated the ability to measure the level of vascular endothelial growth factor (VEGF) in clinical blood plasma samples taken from the breast cancer patients and exhibited excellent resistance to interference from biological species in complex matrices.<sup>189</sup> This sensor configuration

provides a general detection scheme that can be adapted for measurement of a wide range of biomolecules. For example, a SERS sensor has been developed using these guidelines to detect hepatitis B virus DNA with a LOD of about 50 aM, as shown in Figure 12c.<sup>186</sup>

## 6. Conclusions and perspectives

Plasmonics can be used directly for signal transduction or utilized to mediate fluorescence and enhance SERS. Sensors based on plasmon-transduction are well established. In particular, colorimetric sensors are simple and easily constructed. However, this type of sensor has a relatively low sensitivity and is more vulnerable to interference compared to fluorescence and SERS. Fluorescence sensors based on visible-light fluorophores have been widely used in various fields due to their high sensitivity, low-cost, and abundant commercial availability. However, near-infrared fluorophores have a very low quantum yield, limiting their sensitivity and usefulness. This can be overcome by incorporating a plasmonic nanostructure with the near-infrared dye, enhancing the fluorescence. Compared to fluorescence and plasmonic sensors, SERS sensors are relatively new but have an outstanding capability to perform chemical analysis and imaging at larger penetration depths than other optical techniques while maintaining excellent anti-interference properties, allowing *in-vivo* imaging and detection of real-world samples. Fluorescence and colorimetric plasmonic sensing systems can be easily integrated into a compact instrument. In contrast, SERS instruments were historically large in size and expensive, putting a constraint on the application of SERS in point-of-care devices. In the last decade, significant progress has been made to solve this problem. Commercial bench-top or palm-sized Raman readers are available now. The development of plasmon-enhanced SERS technology poises to further speed up the availability of compact SERS sensing systems.

Recently, paper- and fiber-based SERS substrates have become the focus of SERS research because of their flexibility, conformability, efficient uptake of analytes, and efficient transport due to hierarchical vasculature and high specific surface area.<sup>254-257</sup> These novel SERS substrates are also easily integrated into conventional chromatography, microfluidics, and other biological assays, and therefore hold great promise in future SERS applications. In addition, one of the most promising features of future SERS is the capability of multiplexed detection in live animals.<sup>258-261</sup> SERS therefore holds great promise for chemical sensing and *in vivo* biological imaging as plasmonic-based design continues to progress.

In the future, plasmonics will continue to be developed for not only enhancing the sensing signal but also for designing new detection schemes based on fluorescence and SERS devices. To date, many plasmon-involved sensors were constructed on an empirical basis. A “Device-by-Design” fashion is desirable to ensure the continued development of high-performance plasmon-mediated sensors, but this is impossible without first establishing an in-depth understanding

of the underlying theory. The mechanisms of plasmonic transduction and plasmon-enhanced SERS have been already well studied. Although significant progress has been made in understanding the underlying mechanism of plasmon-mediated fluorescence, more systematic studies need to be performed to clarify the confusion on the issue of enhancement versus quenching. The limits of plasmonic sensors can only be pushed once the underlying theory is well understood.

Both LSPR and SPP can be tailored by nanostructured material and architecture, providing great opportunity and flexibility for designing plasmon-enhanced sensors. The success of future plasmon-enhanced sensors directly depends on the effective design of plasmonic materials/architectures and the development of new methods for their fabrication.

## Acknowledgements

Research reported in this publication was supported by the National Institute of Neurological Disorders and Stroke of the National Institutes of Health under Award Number R15NS087515. The content is solely the responsibility of the authors and does not necessarily represent the official views of the National Institutes of Health. This work was also partially supported by a NSF grant (CBET-1336205). Cushing was supported by NSF Research Graduate Fellowship (No. 1102689). The resource and facilities used were partially supported by NSF (EPS 1003907).

## Notes and references

<sup>a</sup>Department of Mechanical and Aerospace Engineering, West Virginia University, Morgantown, WV 26506-6106, USA. E-mail: nick.wu@mail.wvu.edu

<sup>b</sup>Department of Physics and Astronomy, West Virginia University, Morgantown, WV 26506-6315, USA.

- 1 M. R. Jones, K. D. Osberg, R. J. Macfarlane, M. R. Langille and C. A. Mirkin, *Chem. Rev.* 2011, **111**, 3736-3827.
- 2 E. Ringe, J. Zhang, M. R. Langille, K. Sohn, C. Cogley, L. Au, Y. Xia, C. A. Mirkin, J. Huang, L. D. Marks and R. P. Van Duyne, *Mater. Res. Soc. Symp. Proc.*, 2010, **1208**, O10-02.
- 3 E. Ringe, M. R. Langille, K. Sohn, J. Zhang, J. Huang, C. A. Mirkin, R. P. Van Duyne and L. D. Marks, *J. Phys. Chem. Lett.*, 2012, **3**, 1479-1483.
- 4 P. K. Jain and M. A. El-Sayed, *J. Phys. Chem. C*, 2007, **111**, 17451-17454.
- 5 D. W. Brandl, N. A. Mirin and P. Nordlander, *J. Phys. Chem. B*, 2006, **110**, 12302-12310.
- 6 S. K. Ghosh and T. Pal, *Chem. Rev.* 2007, **107**, 4797-4862.
- 7 I. E. Sendroiu, M. E. Warner and R. M. Corn, *Langmuir*, 2009, **25**, 11282-11284.
- 8 K. M. Mayer and J. H. Hafner, *Chem. Rev.*, 2011, **111**, 3828-3857.
- 9 I. Lieberman, G. Shemer, T. Fried, E. M. Kosower and G. Markovich, *Angew. Chem. Int. Ed.*, 2008, **47**, 4855-4857.
- 10 A. J. Haes, S. Zou, G. C. Schatz and R. P. Van Duyne, *J. Phys. Chem. B*, 2004, **108**, 109-116.
- 11 N. W. Ashcroft and D. N. Mermin. *Solid Stat. Physics.* (Cengage Learning, 1976)

- 12 T. W. H. Oates, H. Wormeester, and H. Arwin, *Prog. Surf. Sci.*, 2011, **86**, 328-376.
- 13 J. R. Lackowicz, *Plasmonics*, 2006, **1**, 5-33.
- 14 J. Dostalek and W. Knoll, *Biointerphases*, 2008, **3**, 12-22.
- 15 V. M. Shalaev and S. Kawata, *Nanophotonics with Surface Plasmon*. (Elsevier, 2007).
- 16 Y. Li, K. Zhao, H. Sobhani, K. Bao, and P. Nordlander, *J. Phys. Chem. Lett.*, 2013, **4**, 1352-1357.
- 17 P. Mulvaney, *Langmuir* 1996, **12**, 788-800.
- 18 A.M. Schwartzberg and J.Z. Zhang, *J. Phys. Chem. C*. 2008, **112**, 10323-10337.
- 19 M. Li, S. K. Cushing, J. Zhang, J. Lankford, Z. P. Aguilar, D. Ma and N. Wu, *Nanotechnology*, 2012, **23**, 115501.
- 20 K. A. Willets and R. P. Van Duyne, *Annu. Rev. Phys. Chem.*, 2007, **58**, 267-297.
- 21 K. S. Lee and M. A. El-Sayed, *J. Phys. Chem. B*, 2005, **109**, 20331-20338.
- 22 P. D. Nallathamby, T. Huang and X. H. N. Xu, *Nanoscale*, 2010, **2**, 1715-1722.
- 23 L. Tong, Q. Wei, A. Wei and J. X. Cheng, *Photochem. Photobiol.*, 2009, **85**, 21-32.
- 24 A. J. Haes, C. L. Haynes, A. D. McFarland, G. C. Schatz, R. P. Van Duyne and S. Zou, *MRS Bull.*, 2005, **30**, 368-375.
- 25 M. Li, H. Gou, I. Al-Ogaïdi and N. Wu, *ACS Sustainable Chem. Eng.*, 2013, **1**, 713-723.
- 26 H. Wang, C. S. Levin and N. J. Halas, *J. Am. Chem. Soc.*, 2005, **127**, 14992-14993.
- 27 I. Gryczynski, J. Malicka, Z. Gryczynski, and J. R. Lakowicz, *Anal. Biochem.*, 2004, **324**, 170-182.
- 28 J. R. Lakowicz, *Anal. Biochem.*, 2005, **337**, 171-194.
- 29 C. Sönnichsen, T. Franzl, T. Wilk, G. Von Plessen and J. Feldmann, *Phys. Rev. Lett.*, 2002, **88**, 077402.
- 30 E. Prodan, C. Radloff, N. J. Halas and P. Nordlander, *Science*, 2003, **17**, 419-422.
- 31 A. G. Brolo, *Nat. Photonics*, 2012, **6**, 709-713.
- 32 Y. Liu, and Q. Cheng, *Anal. Chem.*, 2012, **84**, 3179-3186.
- 33 T. Špringer, M. Piliarik and J. Homola, *Anal. Bioanal. Chem.*, 2010, **398**, 1955-1961.
- 34 K. Aslan, P. Holley, L. Davies, J. R. Lakowicz and C. D. Geddes, *J. Am. Chem. Soc.*, 2005, **127**, 12115-12121.
- 35 F. Inci, O. Tokel, S. Wang, U. A. Gurkan, S. Tasoglu, D. R. Kuritzkes and U. Demirci, *ACS Nano*, 2013, **7**, 4733-4745.
- 36 Y. Uludag and I. E. Tothill, *Anal. Chem.*, 2012, **84**, 5898-5904.
- 37 O. R. Bolduc and J. F. Masson, *Anal. Chem.*, 2011, **83**, 8057-8062.
- 38 A. J. Haes, S. Zou, J. Zhao, G. C. Schatz and R. P. Van Duyne, *J. Am. Chem. Soc.*, 2006, **128**, 10905-10914.
- 39 J. Zhao, L. Jensen, J. Sung, S. Zou, G. C. Schatz and R. P. Van Duyne, *J. Am. Chem. Soc.*, 2007, **129**, 7647-7656.
- 40 W. C. Law, K. T. Yong, A. Baev and P. N. Prasad, *ACS Nano*, 2011, **5**, 4858-4864.
- 41 J. Li, S. K. Cushing, P. Zheng, F. Meng, D. Chu and N. Q. Wu, *Nat. Commun.*, 2013, **4**, 2651.
- 42 T. W. Ebbesen, H. J. Lezec, H. F. Ghaemi, T. Thio and P. A. Wolff, *Nature*, 1998, **391**, 667-669.
- 43 A. G. Brolo, R. Gordon, B. Leathem and K. L. Kavanagh, *Langmuir* 2004, **20**, 4813-4815.
- 44 N. Liu, T. Weiss, M. Mesch, L. Langguth, U. Eigenthaler, M. Hirscher, C. Sönnichsen and H. Giessen, *Nano Lett.*, 2009, **10**, 1103-1107.
- 45 A. De Leebeeck, L. K. S. Kumar, V. de Lange, D. Sinton, R. Gordon and A. G. Brolo, *Anal. Chem.*, 2007, **79**, 4094-4100.
- 46 H. Im, J. N. Sutherland, J. A. Maynard and S.-H. Oh, *Anal. Chem.*, 2012, **84**, 1941-1947.
- 47 A. Lesuffleur, H. Im, N. C. Lindquist, K. S. Lim and S.-H. Oh, *Opt. Express*, 2008, **16**, 219-224.
- 48 L. Pang, G. M. Hwang, B. Slutsky, Y. Fainman, *App. Phys. Lett.*, 2007, **91**, 123112.
- 49 M. Lahav, A. Vaskevich and I. Rubinstein, *Langmuir*, 2004, **20**, 7365-7367.
- 50 M. D. Malinsky, K. L. Kelly, G. C. Schatz and R. P. Van Duyne, *J. Am. Chem. Soc.*, 2001, **123**, 1471-1482.
- 51 C. Gao, Z. Lu, Y. Liu, Q. Zhang, M. Chi, Q. Cheng and Y. Yin, *Angew. Chem. Int. Ed.*, 2012, **51**, 5629-5633.
- 52 Z. D. Liu, Y. F. Li, J. Ling and C. Z. Huang, *Environ. Sci. Technol.*, 2009, **43**, 5022-5027.
- 53 R. Méjard, J. Dostálek, C.-J. Huang, H. Griesser and B. Thierry, *Opt. Mater.*, 2013, **35**, 2507-2513.
- 54 M. Vala, S. Etheridge, J.A. Roach and J. Homola, *Sens. Act. B*, 2009, **139**, 59-63.
- 55 D. Sarid, *Phys. Rev. Lett.*, 1981, **47**, 1927-1930.
- 56 J. Homola, *Anal. Bioanal. Chem.* 2003, **377**, 528-539.
- 57 T. Kim, K. Lee, M. S. Gong, and S. W. Joo, *Langmuir*, 2005, **21**, 9524-9528.
- 58 H. N. Kim, W. X. Ren, J. S. Kim and J. Yoon, *Chem. Soc. Rev.*, 2012, **41**, 3210-3244.
- 59 H. Liang, H. Zhao, D. Rossouw, W. Wang, H. Xu, G. A. Botton and D. Ma, *Chem. Mater.*, 2012, **24**, 2339-2346.
- 60 L. He, M. D. Musick, S. R. Nicewarner, F. G. Salinas, S. J. Benkovic, M. J. Natan and C. D. Keating, *J. Am. Chem. Soc.*, 2000, **122**, 9071-9077.
- 61 J. M. Slocik, J. S. Zabinski, D. M. Phillips and R. R. Naik, *Small*, 2008, **4**, 548-551.
- 62 J. Zhang, L. Wang, D. Pan, S. Song, F. Y. Boey, H. Zhang and C. Fan, *Small*, 2008, **4**, 1196-1200.
- 63 Y. Zhou, S. Wang, K. Zhang and X. Jiang, *Angew. Chem. Int. Ed.*, 2008, **47**, 7454-7456.
- 64 Y. Jiang, H. Zhao, N. Zhu, Y. Lin, P. Yu and L. Mao, *Angew. Chem. Int. Ed.*, 2008, **47**, 8601-8604.
- 65 W. L. Daniel, M. S. Han, J. S. Lee and C. A. Mirkin, *J. Am. Chem. Soc.*, 2009, **131**, 6362-6363.
- 66 C. J. Yu and W. L. Tseng, *Langmuir*, 2008, **24**, 12717-12722.
- 67 B. Kong, A. Zhu, Y. Luo, Y. Tian, Y. Yu and G. Shi, *Angew. Chem. Int. Ed.*, 2011, **50**, 1837-1840.
- 68 J. J. Storhoff, R. Elghanian, R. C. Mucic, C. A. Mirkin and R. L. Letsinger, *J. Am. Chem. Soc.*, 1998, **120**, 1959-1964.
- 69 H. Li and L. Rothberg, *Proc. Nat. Acad. Sci. USA*, 2004, **101**, 14036-14039.
- 70 J. Zhang, L. Wang, D. Pan, S. Song, F. Y. Boey, H. Zhang and C. Fan, *Small*, 2008, **4**, 1196-1200.
- 71 W. Xu, X. Xue, T. Li, H. Zeng and X. Liu, *Angew. Chem. Int. Ed.*, 2009, **48**, 6849-6852.
- 72 R. Elghanian, J. J. Storhoff, R. C. Mucic, R. L. Letsinger and C. A. Mirkin, *Science*, 1997, **277**, 1078-1081.

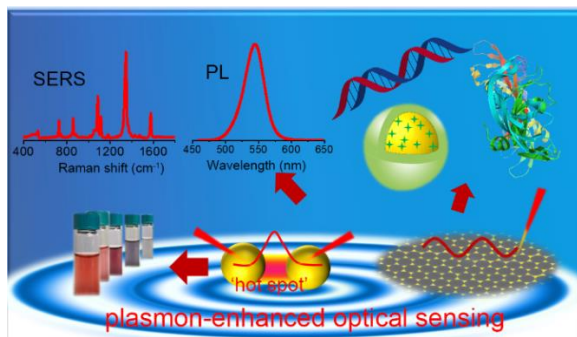
- 73 Y. Kim, R. C. Johnson and J. T. Hupp, *Nano Lett.*, 2001, **1**, 165-167.
- 74 J. J. Storhoff, R. Elghanian, R. C. Mucic, C. A. Mirkin and R. L. Letsinger, *J. Am. Chem. Soc.*, 1998, **120**, 1959-1964.
- 75 J. S. Lee, M. S. Han and C. A. Mirkin, *Angew. Chem. Int. Ed.*, 2007, **119**, 4171-4174.
- 76 D. A. Giljohann, D.S. Seferos, W. L. Daniel, M.D. Massich, P. C. Patel and C. A. Mirkin, *Angew. Chem. Int. Ed.*, 2010, **49**, 3280 – 3294.
- 77 X. Xue, F. Wang and X. Liu, *J. Am. Chem. Soc.*, 2008, **130**, 3244-3245.
- 78 X. Xu, W. L. Daniel, W. Wei and C. A. Mirkin, *Small*, 2010, **6**, 623-626.
- 79 T. Li, L. Shi, E. Wang and S. Dong, *Chem.-A Europ. J.*, 2009, **15**, 3347-3350.
- 80 J. Yguerabide and E. E. Yguerabide, *Anal. Biochem.*, 1998, **262**, 157-176.
- 81 Y. Sun and Y. Xia, *Anal. Chem.*, 2002, **74**, 5297-5305.
- 82 J. Liu, D. Mazumdar and Y. Lu, *Angew. Chem. Int. Ed.*, 2006, **45**, 7955-7959.
- 83 H. Xu, X. Mao, Q. Zeng, S. Wang, A.-N. Kawde and G. Liu, *Anal. Chem.*, 2008, **81**, 669-675.
- 84 X. Gao, H. Xu, M. Baloda, A. S. Gurung, L. P. Xu, T. Wang, X. Zhang and G. Liu, *Biosens. Bioelectro.*, 2014, **54**, 578-584.
- 85 C. S. Thaxton and C. A. Mirkin, *Nat. Biotech.*, 2005, **23**, 681-682.
- 86 C. Sönnichsen, B. M. Reinhard, J. Liphardt and A. P. Alivisatos, *Nat. Biotech.*, 2005, **23**, 741-745.
- 87 Y. Choi, Y. Park, T. Kang and L. P. Lee, *Nat. Nanotechnol.*, 2009, **4**, 742-746.
- 88 Y. Choi, T. Kang and L. P. Lee, *Nano Lett.*, 2008, **9**, 85-90.
- 89 G. L. Liu, Y. T. Long, Y. Choi, T. Kang and L. P. Lee, *Nat. Methods*, 2007, **4**, 1015-1017.
- 90 W. G. Qu, B. Deng, S. L. Zhong, H. Y. Shi, S. S. Wang and A. W. Xu, *Chem. Comm.*, 2011, **47**, 1237-1239.
- 91 J. Du, L. Jiang, Q. Shao, X. Liu, R. S. Marks, J. Ma and Chen, X. *Small*, 2013, **9**, 1467-1481.
- 92 J. W. Attridge, P. B. Daniels, J. K. Deacon, G. A. Robinson and G. P. Davidson, *Biosens. Bioelectro.*, 1991, **6**, 201-214.
- 93 A. E. Vasdekis and G. P. J. Laporte, *Int. J. Mol. Sci.*, 2011, **12**, 5135-5156.
- 94 A. Kinkhabwala, Z. Yu, S. Fan, Y. Avlasevich, K. Müllen and W. E. Moerner, *Nat. Photonics*, 2009, **3**, 654 – 657.
- 95 E. Fort and S. Gresillon, *J. Phys. D: Appl. Phys.*, 2008, **41**, 013001.
- 96 J. R. Lakowicz, K. Ray, M. Chowdhury, H. Szmecinski, Y. Fu, J. Zhang and K. Nowaczyk, *Analyst*, 2008, **133**, 1308-1346.
- 97 M. Bauch, K. Toma, M. Toma, Q. Zhang and J. Dostalek, *Plasmonics*, 2014, DOI 10.1007/s11468-013-9660-5.
- 98 J. R. Lakowicz. *Principles of Fluorescence Spectroscopy*. (Springer Academic, 2006).
- 99 Y. C. Tsai, C. F. Lin, and J. W. Chang, *Opt. Rev.*, 2009, **16**, 347-350.
- 100 H. Mertens, A. F. Koenderink and A. Polman, *Phys. Rev. B.*, 2007, **76**, 115123.
- 101 J. B. Khurgin and G. Sun, *J. Opt. Soc. Am. B.*, 2009, **26**, B83-B95.
- 102 G. Sun, J. B. Khurgin, and C. C. Yang, *Appl. Phys. Lett.*, 2009, **95**, 171103.
- 103 H. F. Arnoldus and T. F. George, *J. Chem. Phys.*, 1987, **87**, 4263.
- 104 P. Bharadwaj and L. Novotny, *Opt. Express*, 2007, **15**, 14271
- 105 K. A. Kang, J. Wang, J. B. Jasinski and S. Achilefu, *J. Nanobiotechnology*, 2011, **9**, 16
- 106 T. Ming, H. Chen, R. Jiang, Q. Li and J. Wang, *J. Phys. Chem. Lett.*, 2012, **3**, 191-202.
- 107 S. M. Morton, D. W. Silverstein and L. Jensen, *Chem. Rev.*, 2011, **111**, 3962-3994.
- 108 D. Cheng and Q. H. Xu, *Chem. Comm.*, 2007, **3**, 248-250.
- 109 F. Yu, B. Persson, S. Löfås and W. Knoll, *J. Am. Chem. Soc.*, 2004, **126**, 8902-8903.
- 110 Y. Shan, J. J. Xu and H. Y. Chen, *Chem. Comm.*, 2009, **8**, 905-907.
- 111 P. Bharadwaj and L. Novotny, *Opt. Express*, 2007, **15**, 14266-14274.
- 112 H. Naiki, A. Masuhara, S. Masuo, T. Onodera, H. Kasai and H. Oikawa, *J. Phys. Chem. C*, 2012, **117**, 2455-2459.
- 113 Y. Chen, K. Munechika and D. S. Ginger, *Nano Lett.*, 2007, **7**, 690-696.
- 114 P. P. Pompa, L. Martiradonna, A. Della Torre, F. Della Sala, L. Manna, De Vittorio, M., F. Calabi, R. Cingolani and R. Rinaldi, *Nat. Nanotechnol.*, 2006, **1**, 126-130.
- 115 A. Kinkhabwala, Z. Yu, S. Fan, Y. Avlasevich, K. Müllen and W. E. Moerner, *Nat. Photonics*, 2009, **3**, 654-657.
- 116 G. Sun and J. B. Khurgin, *Phys. Rev. A.*, 2012, **85**, 063410.
- 117 S. Lal, N. K. Grady, J. Kundu, C. S. Levin, J. B. Lassiter and N. J. Halas, *Chem. Soc. Rev.*, 2008, **37**, 898-911.
- 118 R. Wilson and D. V. Nicolau, *Angew. Chem.*, 2011, **123**, 2199-2202.
- 119 Y. Li, J. Sun, L. Wu, J. Ji, X. Sun, and Y. Qian, *Biosens. Bioelectro.*, 2014, **62**, 255-260.
- 120 H. Li, C. Y. Chen, X. Wei, W. Qiang, Z. Li, Q. Cheng and D. Xu, *Anal. Chem.*, 2012, **84**, 8656-8662.
- 121 H. Li, W. Qiang, M. Vuki, D. Xu and H. Y. Chen, *Anal. Chem.*, 2011, **83**, 8945-8952.
- 122 R. Robelek, L. Niu, E. L. Schmid and W. Knoll, *Anal. Chem.*, 2004, **76**, 6160-6165.
- 123 H. Cho, E. C. Yeh, R. Sinha, T. A. Laurence, J. P. Bearinger and L. P. Lee, *ACS Nano*, 2012, **6**, 7607-7614.
- 124 J. Zhang, Y. Tang, K. Lee and M. Ouyang, *Science*, 2010, **327**, 1634-1638.
- 125 J. S. Lee, E. V. Shevchenko and D. V. Talapin, *J. Am. Chem. Soc.*, 2008, **130**, 9673-9675.
- 126 H. Li, C. Y. Chen, X. Wei, W. Qiang, Z. Li, Q. Cheng and D. Xu, *Anal. Chem.*, 2012, **84**, 8656-8662.
- 127 P. Sharma, M. Kakkar, A. Ganguli, A. Bhasin and C. R. Suri, *Analyst*, 2013, **138**, 4312-4320
- 128 S. Khatua, P. M. R. Paulo, H. Yuan, A. Gupta and P. Z. M. Orrit, *ACS Nano*, 2014, **8**, 4440-4449.
- 129 F. Tam, G. P. Goodrich, B. R. Johnson and N. J. Halas, *Nano Lett.*, 2007, **7**, 496-501.
- 130 C. Xiao, Z. Cao, J. Deng, Z. Huang, Z. Xu, J. Fu and L. Yobas, *J. P. Hu, L. L. Zheng, L. Zhan, J. Y. Li, S. J. Zhen, H. Liu, L. F. Luo, G. F. Xiao and C. Z. Huang, Anal. Chim. Acta*, 2013, **787**, 239-245.
- 132 L. Lu, Y. Qian, L. Wang, K. Ma and Y. Zhang, *ACS App. Mater. Interf.*, 2014, **6**, 1944-1950.
- 133 E. Hwang, I. I. Smolyaninov and C. C. Davis, *Nano Lett.*, 2010, **10**, 813-820.
- 134 Y.-F. Chang, J.-S. Yu, Y.-T. Chang, S.-Y. Chang, L.-C. Su, C.-C. Wu, Y.-S. Chang, C.-S. Lai, C. Chou, *Biosens. Bioelectro.*, 2013, **41**, 232-237.

- 135 C.-H. Chao and Y.-F. Chang, H.-C. Chen, L.-Y. Lin, P.-C. Yu, Y.-S. Chang, Y.-J. Lee and C. Chou, *Sens. Act. B*, 2012, **173**, 184-190.
- 136 H. Li, C. Y. Chen, X. Wei, W. Qiang, Z. Li, Q. Cheng, D. Xu, *Anal. Chem.*, 2012, **84**, 8656-8662.
- 137 R. Nooney, A. Clifford, X. Leguevel, O. Stranik, C. McDonagh and B. D. Maccraith, *Anal. Bioanal. Chem.*, 2010, **396**, 1127-1134.
- 138 K. Aslan and T. A.J. Grell, *Clin. Chem.*, 2011, **57**, 746-752.
- 139 L. Touahir, E. Galopin, R. Boukherroub, A. C. Gouget-Laemmel, J. N. Chazalviel, F. Ozanam and S. Szunerits, *Biosens. Bioelectro.*, 2010, **25**, 2579-2585.
- 140 F. Xie, J. S. Pang, A. Centeno, M. P. R., D. J. Riley, N. M. Alford, *Nano Res.*, 2013, **6**, 496-510.
- 141 A. G. Brolo, S. C. Kwok, M. G. Moffitt, R. Gordon, J. Riordon, K. L. Kavanagh, *J. Am. Chem. Soc.*, 2005, **127**, 14936-14941.
- 142 S. H. Cao, W. P. Cai, Q. Liu and Y. Q. Li, *Ann. Rev. Anal. Chem.*, 2012, **5**, 317-336.
- 143 J. Malicka, I. Gryczynski, Z. Gryczynski and J. R. Lakowicz, *Anal. Chem.* 2003, **75**, 6629-6633
- 144 T. T. Xie, Q. Liu, W. P. Cai, Z. Chen and Y. Q. Li, *Chem. Commun.* 2009, **45**, 3190-3192.
- 145 E. Matveeva, Z. Gryczynski, I. Gryczynski and J. R. Lakowicz, *J. Immunol. Methods*, 2004, **286**, 133-140.
- 146 A. Kasry and W. Knoll, *Appl. Phys. Lett.*, 2006, **89**, 101106.
- 147 C. J. Huang, A. Sessitsch, J. Dostalek, W. Knoll, *Anal. Chem.*, 2011, **83**, 674-677.
- 148 Y. Wang, J. Dostalek and W. Knoll, *Biosens. Bioelectro.*, 2009, **24**, 2264-2267.
- 149 Y. Wang, A. Brunsen, U. Jonas, J. Dostalek and W. Knoll, *Anal. Chem.*, 2009, **81**, 9625-9632.
- 150 C. Zhang, Y. Yuan, S. Zhang, Y. Wang and Z. Liu, *Angew. Chem. Int. Ed.*, 2011, **50**, 6851-6854.
- 151 H. Takanaga, B. Chaudhuri and W. B. Frommer, *Biochim. Biophys. Acta-Biomembr.*, 2008, **1778**, 1091-1099.
- 152 J. L. Vinkenburg, T. H. Evers, S. W. Reulen, E. W. Meijer and M. Merkx, *ChemBioChem*, 2007, **8**, 1119-1121.
- 153 K. Kikuchi, H. Takakusa and T. Nagano, *TrAC Trends Anal. Chem.*, 2004, **23**, 407-415.
- 154 B. G. Fuller, M. A. Lampson, E. A. Foley, S. Rosasco-Nitcher, K. V. Le, P. Tobelmann, D. L. Brautigam, P. T. Stukenberg and T. M. Kapoor, *Nature*, 2008, **453**, 1132-1136.
- 155 M. Fehr, S. Okumoto, K. Deuschle, I. Lager, L. L. Looger, J. Persson, L. Kozhukh, S. Lalonde and W. B. Frommer, *Biochem. Soc. Trans.*, 2005, **33**, 287-290.
- 156 M. A. Rizzo, G. H. Springer, B. Granada and D. W. Piston, *Nat. Biotechnol.*, 2004, **22**, 445-449.
- 157 X. Zhang, Y. Xiao and X. Qian, *Angew. Chem. Int. Ed.*, 2008, **47**, 8025-8029.
- 158 J. L. Vinkenburg, T. J. Nicolson, E. A. Bellomo, M. S. Koay, G. A. Rutter and M. Merkx, *Nat. Method.*, 2009, **6**, 737-740.
- 159 I. L. Medintz, A. R. Clapp, H. Mattoussi, E. R. Goldman, B. Fisher and J. M. Mauro, *Nat. Mater.*, 2003, **2**, 630-638.
- 160 A. Woehler, J. Wlodarczyk and E. Neher, *Biophys. J.*, 2010, **99**, 2344-2354.
- 161 J. Zhang, Y. Fu, M. H. Chowdhury and J. R. Lakowicz, *Nano Lett.*, 2007, **7**, 2101-2107
- 162 M. Kondon, J. Kim, N. Udawatte and D. Lee, *J. Phys. Chem. C*, 2008, **112**, 6695-6699.
- 163 M. Li, S. K. Cushing, Q. Wang, X. Shi, L. A. Hornak, Z. Hong and N. Wu, *J. Phys. Chem. Lett.*, 2011, **2**, 2125-2129.
- 164 M. Lessard-Viger, M. Rioux, L. Rainville and D. Boudreau, *Nano Lett.*, 2009, **9**, 3066-3071.
- 165 J. R. Lakowicz, Y. Shen, S. D'Auria, J. Malicka, J. Fang, Z. Gryczynski and I. Gryczynski, *Anal. Biochem.*, 2002, **301**, 261-277.
- 166 J. Y. Chang, T. G. Kim and Y. M. Sung, *Nanotechnology*, 2011, **22**, 425708.
- 167 A. Manivel and S. Anandan, *Colloids Surf. A: Physicochem. Eng. Aspects*, 2012, **395**, 38-45.
- 168 J. Zhang, Y. Fu, M. H. Chowdhury and J. R. Lakowicz, *J. Phys. Chem. C*, 2007, **111**, 11784-11792.
- 169 F. Reil, U. Hohenester, J. R. Krenn and A. Leitner, *Nano Lett.*, 2008, **8**, 4128-4133.
- 170 P. R. Selvin, *Nat. Struct. Bio.*, 2000, **7**, 730-734.
- 171 X. Zhang, C. A. Marocico, M. Lunz, V. A. Gerard, Y. K. Guñko, V. Lesnyak, N. Gaponik, A. S. Susha, A. L. Rogach and A. L. Bradley, *ACS Nano*, 2012, **6**, 9283-9290.
- 172 C. S. Yun, A. Javier, T. Jennings, M. Fisher, S. Hira, S. Peterson, B. Hopkins, N. O. Reich and Strouse, G. F. *J. Am. Chem. Soc.*, 2005, **127**, 3115-3119.
- 173 M. Li, Q. Wang, X. Shi, L. A. Hornak and N. Q. Wu, *Anal. Chem.*, 2011, **83**, 7061-7065.
- 174 E. Oh, M. Y. Hong, D. Lee, S. H. Nam, H. C. Yoon and H. S. Kim, *J. Am. Chem. Soc.*, 2005, **127**, 3270-3271.
- 175 G. K. Darbha, A. Ray and P. C. Ray, *ACS Nano*, 2007, **1**, 208-214.
- 176 T. Pons, I. L. Medintz, K. E. Sapsford, S. Higashiyama, A. F. Grimes, D. S. English and H. Mattoussi, *Nano Lett.*, 2007, **7**, 3157-3164.
- 177 J. Ling and C. Z. Huang, *Anal. Method*, 2010, **2**, 1439-1447.
- 178 J. Zhang, Y. Fu and J. R. Lakowicz, *J. Phys. Chem. C*, 2007, **111**, 50-56.
- 179 T. Ozel, P. L. Hernandez Martinez, E. Mutlugun, O. Akin, S. Nizamoglu, I. O. Ozel, Q. Zhang, Q. Xiong and H. V. Demir, *Nano Lett.*, 2013, **13**, 3065-3072
- 180 L. Zhao, T. Ming, L. Shao, H. Chen, and J. Wang, *J. Phys. Chem. C.*, 2012, **116**, 8287-8296.
- 181 V. K. Komarala, A. L. Bradley, Y. P. Rakovich, S. J. Byrne, Y. K. Gunko, and A. L. Rogach, *Appl. Phys. Lett.*, 2008, **93**, 123102.
- 182 H. Li, M. Wang, C. Wang, W. Li, W. Qiang and D. Xu, *Anal. Chem.*, 2013, **85**, 4492-4499.
- 183 Z. Zhou, H. Huang, Y. Chen, F. Liu, C. Huang and N. Li, *Biosens. Bioelectro.*, 2014, **52**, 367-373.
- 184 M. Li, R. Li, C. M. Li and N. Wu, *Front. Biosci.*, 2011, **S3**, 1308-1331
- 185 K. Kneipp, Y. Wang, H. Kneipp, L. T. Perelman, I. Itzkan, R. R. Dasari and M. S. Feld, *Phys. Rev. Lett.*, 1997, **78**, 1667.
- 186 M. Li, S. K. Cushing, H. Liang, S. Suri, D. Ma, N. Wu, *Anal. Chem.*, 2013, **85**, 2072-2078.
- 187 M. Li, J. Zhang, S. Suri, L. J. Sooter, D. Ma and N. Wu, *Anal. Chem.*, 2012, **84**, 2837-2842.
- 188 M. Li, S. K. Cushing, J. Zhang, J. Lankford, Z. P. Aguilar, D. Ma and N. Wu, *Nanotechnology*, 2012, **23**, 115501.
- 189 M. Li, S. K. Cushing, J. Zhang, S. Suri, R. Evans, W. P. Petros, L. F. Gibson, D. Ma, Y. Liu and N. Wu, *ACS Nano*, 2013, **7**, 4967-4976

- 190 J. Yang, M. Palla, F. G. Bosco, T. Rindzevicius, T. S. Alstrøm, M. S. Schmidt, A. Booisens, J. Ju and Q. Lin, *ACS Nano*, 2013, **7**, 5350–5359.
- 191 S. Zong, Z. Wang, H. Chen, J. Yang and Y. Cui, *Anal. Chem.*, 2013, **85**, 2223–2230.
- 192 Y. Wang, B. Yan and L. Chen, *Chem. Rev.*, 2012, **113**, 1391–1428.
- 193 Y. S. Michael, H. Xu, S. G. Penn and R. Cromer, *Nanomedicine-UK*, 2007, **2**, 725–734.
- 194 S. D. Hudson and G. Chumanov, *Anal. Bioanal. Chem.*, 2009, **394**, 679–686.
- 195 Y. Wang, B. Yan and L. Chen, *Chem. Rev.*, 2012, **113**, 1391–1428.
- 196 E. C. Le Ru, E. Blackie, M. Meyer and P. G. Etchegoin, *J. Phys. Chem. C*, 2007, **111**, 13794–13803.
- 197 J. Chen, B. Shen, G. Qin, X. Hu, L. Qian, Z. Wang, S. Li, Y. Ren and L. Zuo, *J. Phys. Chem. C*, 2012, **116**, 3320–3328.
- 198 S. Y. Lee, L. Hung, G. S. Lang, J. E. Cornett, I. D. Mayergoyz and O. Rabin, *ACS Nano*, 2010, **4**, 5763–5772.
- 199 F. S. Ameer, W. Hu, S. M. Ansa, K. Siriwardana, W. E. Collier, S. Zou and D. Zhang, *J. Phys. Chem. C*, 2013, **117**, 3483–3488.
- 200 H. Xu, X. H. Wang, M. P. Persson, and H.Q. Xu, *Phys. Rev. Lett.*, 2004, **93**, 243002.
- 201 S. D. Christesen, *Appl. Spectro.*, 1988, **42**, 318–321.
- 202 E. Papadopoulou and S. E. Bell, *Angew. Chem. Int. Ed.*, 2011, **50**, 9058–9061.
- 203 C. Otto, T. J. J. Van den Tweel, F. F. M. De Mul and J. Greve, *J. Raman Spectrosc.*, 1986, **17**, 289–298.
- 204 A. Barhoumi, D. Zhang, F. Tam and N. J. Halas, *J. Am. Chem. Soc.*, 2008, **130**, 5523–5529.
- 205 A. Barhoumi and N. J. Halas, *J. Am. Chem. Soc.*, 2010, **132**, 12792–12793.
- 206 N. H. Kim, S. J. Lee and M. Moskovits, *Nano Lett.*, 2010, **10**, 4181–4185.
- 207 M. Mulvihill, A. Tao, K. Benjauthrit, J. Arnold and P. Yang, *Angew. Chem.*, 2008, **120**, 6556–6560.
- 208 R. A. Alvarez-Puebla and L. M. Liz-Marzán, *Angew. Chem. Int. Ed.*, 2012, **51**, 11214–11223.
- 209 S. L. Kleinman, R. R. Frontiera, A. I. Henry, J. A. Dieringer and R. P. Van Duyne, *Phys. Chem. Chem. Phys.*, 2013, **15**, 21–36.
- 210 L. Tong, M. Righini, M. U. Gonzalez, R. Quidant and M. Käll, *Lab Chip*, 2009, **9**, 193–195.
- 211 S. Lee, J. Choi, L. Chen, B. Park, J. B. Kyong, G. H. Seong, J. Choo, Y. Lee, K. H. Shin, E. K. Lee, S. W. Joo and K. H. Lee, *Anal. Chim. Acta*, 2007, **590**, 139–144.
- 212 C. E. Talley, L. Jusinski, C. W. Hollars, S. M. Lane and T. Huser, *Anal. Chem.*, 2004, **76**, 7064–7068.
- 213 J. Duan, M. Yang, Y. Lai, J. Yuan and J. Zhan, *Anal. Chim. Acta*, 2012, **723**, 88–93.
- 214 Ž. Krpetić, L. Guerrini, I. A. Larmour, J. Reglinski, K. Faulds and D. Graham, *Small*, 2012, **8**, 707–714.
- 215 F. Toderas, M. Baia, L. Baia and S. Astilean, *Nanotechnology*, 2007, **18**, 255702.
- 216 S. S. Dasary, A. K. Singh, D. Senapati, H. Yu and P. C. Ray, *J. Am. Chem. Soc.*, 2009, **131**, 13806–13812.
- 217 W. Ma, M. Sun, L. Xu, L. Wang, H. Kuang and C. Xu, *Chem. Commun.*, 2013, **49**, 4989–4991.
- 218 I. Al-Ogaidi, H. Gou, A. K. Al-kazaz, Z. Aguilar, A. K. Melconian, P. Zheng and N. Q. Wu, *Anal. Chim. Acta*, 2014, **811**, 76–80.
- 219 L. Qin, S. Park and C. A. Mirkin, *Science*, 2005, **309**, 113–115.
- 220 M. L. Pedano, S. Li, G. C. Schatz and C. A. Mirkin, *Angew. Chem. Int. Ed.*, 2010, **49**, 78–82.
- 221 W. Liu, Z. Zhu, K. Deng, Z. Li, Y. Zhou, H. Qiu, Y. Gao, S. Che and Z. Tang, *J. Am. Chem. Soc.*, 2013, **135**, 9659–9664.
- 222 M. Shanthil, R. Thomas, R. S. Swathi and K. George Thomas, *J. Phys. Chem. Lett.*, 2012, **3**, 1459–1464.
- 223 S. P. Mulvaney, M. D. Musick, C. D. Keating and M. J. Natan, *Langmuir*, 2003, **19**, 4784–4790.
- 224 C. Fernández-López, C. Mateo-Mateo, R. A. Álvarez-Puebla, J. Pérez-Juste, I. Pastoriza-Santos and L. M. Liz-Marzán, *Langmuir*, 2009, **25**, 13894–13899.
- 225 W. E. Doering and S. Nie, *Anal. Chem.*, 2003, **75**, 6171–6176.
- 226 X. M. Qian and S. M. Nie, *Chem. Soc. Rev.* 2008, **37**, 912–920.
- 227 C. Wang, Y. Chen, T. Wang, Z. Ma and Z. Su, *Adv. Funct. Mater.*, 2008, **18**, 355–361.
- 228 L. L. Tay, P. J. Huang, J. Tanha, S. Ryan, X. Wu, J. Hulse and L. K. Chau, *Chem. Commun.*, 2012, **48**, 1024–1026.
- 229 B. Küstner, M. Gellner, M. Schütz, F. Schöppler, A. Marx, P. Ströbel, P. Adam, C. Schmuck and S. Schlücker, *Angew. Chem. Int. Ed.*, 2009, **48**, 1950–1953.
- 230 J. Song, J. Zhou and H. Duan, *J. Am. Chem. Soc.*, 2012, **134**, 13458–13469.
- 231 S. Zong, Z. Wang, H. Chen, J. Yang and Y. Cui, *Anal. Chem.*, 2013, **85**, 2223–2230.
- 232 X. Lu, D. R. Samuelson, Y. Xu, H. Zhang, S. Wang, B. A. Rasco, J. Xu and M. E. Konkel, *Anal. Chem.*, 2013, **85**, 2320–2327.
- 233 J. H. Park, G. von Maltzahn, L. L. Ong, A. Centrone, T. A. Hatton, E. Ruoslahti, S. N. Bhatia and M. J. Sailor, *Adv. Mater.*, 2010, **22**, 880–885.
- 234 X. Qian, X. H. Peng, D. O. Ansari, Q. Yin-Goen, G. Z. Chen, D. M. Shin, L. Yang, A. N. Young, M. D. Wang and S. Nie, *Nat. Biotechnol.*, 2007, **26**, 83–90.
- 235 R. G. Freeman, K. C. Grabar, K. J. Allison, R. M. Bright, J. A. Davis, A. P. Guthrie, M. B. Hommer, M. A. Jackson, P. C. Smith, D. G. Walter, M. J. Natan, *Science*, 1995, **267**, 1629–1632.
- 236 S.-Y. Chu, Y.-W. Huang and Y.-P. Zhao, *Appl. Spectro.*, 2008, **62**, 922–931.
- 237 L. A. Dick, A. D. McFarland, C. L. Haynes and R. P. Van Duyne, *J. Phys. Chem. B*, 2002, **106**, 853–860.
- 238 S. K. Cushing, L. A. Hornak, J. Lankford, Y. Liu and N.Q. Wu, *Appl. Phys. A*, 2011, **103**, 955–958.
- 239 X. Zhang, M. A. Young, O. Lyandres and R. P. Van Duyne, *J. Am. Chem. Soc.*, 2005 **127**, 4484–4449.
- 240 T. R. Jensen, M. D. Malinsky, C. L. Haynes and R. P. Van Duyne, *J. Phys. Chem. B*, 2000, **104**, 10549–10556.
- 241 C. L. Haynes and R. P. Van Duyne, *J. Phys. Chem. B*, 2003, **107**, 7426–7433.
- 242 A. D. McFarland, M. A. Young, J. A. Dieringer and R. P. Van Duyne, *J. Phys. Chem. B*, 2005, **109**, 11279–11285.
- 243 N. A. Hatab, C. -H. Hsueh, A. L. Gaddis, S. T. Retterer, J. -H. Li, G. Eres, Z. Y. Zhang, B. H. Gu, *Nano Lett.*, 2010, **10**, 4952–4955.
- 244 A. G. Brolo, E. Arctander, R. Gordon, B. Leathem and K. L. Kavanagh, *Nano Lett.*, 2004, **4**, 2015–2018.

- 245 Q. Li, Z. Yang, B. Ren, H. Xu and Z. Tian, *J. Nanosci. Nanotechnol.*, 2010, **10**, 7188-7191.
- 246 X. Xuan, S. Xu, Y. Liu, H. Li, W. Xu and J. R. Lombardi, *J. Phys. Chem. Lett.*, 2012, **3**, 2773-2778.
- 247 G. Braun, S. J. Lee, M. Dante, T.-Q. Nguyen, M. Moskovits and N. Reich, *J. Am. Chem. Soc.*, 2007, **129**, 6378-6379.
- 248 J.-M. Li, W.-F. Ma, L.-J. You, J. Guo, J. Hu and C.-C. Wang, *Langmuir*, 2013, **29**, 6147-6155.
- 249 W. Ruan, W. Ji, X. Xue, Y. Cui, L. Chen, T. Zhou, L. Niu, X. Li, J. Zhang and B. Zhao, *J. Raman Spectrosc.*, 2011, **42**, 1492-1496.
- 250 K. K. Strelau, R. Kretschmer, R. Möller, W. Fritzsche and J. Popp, *Anal. Bioanal. Chem.*, 2009, 396, 1381-1384.
- 251 H. Hwang, H. Chon, J. Choo and J.-K. Park, *Anal. Chem.*, 2010, **82**, 7603-7610.
- 252 H. T. Ngo, H.-N. Wang, T. Burke, G. S. Ginsburg and T. Vo-Dinh, *Anal. Bioanal. Chem.*, 2014, **406**, 3335-3344.
- 253 W. J. Cho, Y. Kim and J. K. Kim, *ACS Nano*, 2012, **6**, 249-255.
- 254 W. W. Yu and I. M. White, *Analyst*, 2013, **138**, 1020-1025.
- 255 C. H. Lee, L. Tian and S. Singamaneni, *ACS Appl. Mater. Interf.*, 2010, **2**, 3429-3535.
- 256 C. H. Lee, M. E. Hankus, L. Tian, P. M. Pellegrino and S. Singamaneni, *Anal. Chem.*, 2011, **83**, 8953-8958.
- 257 S. H. Chang, J. Nyagilo, J. Wu, Y. Hao, D. P. Davé, *Plasmonics*, 2012, **7**, 501-508.
- 258 N. Guarrotxena and G. C. Bazan, *Adv. Mater.*, 2014, **26**, 1941-1946.
- 259 H. K. Lee, Y. H. Lee, I. Y. Phang, J. Wei, Y. E. Miao, T. Liu and X. Y. Ling, *Angew. Chem.*, 2014, **126**, 5154-5158.
- 260 M. Li, J. Lu, J. Qi, F. Zhao, J. Zeng, J. C. Yu and W. C. Shih, *J. Biomed. Opt.*, 2014, **19**, 50501-50501.
- 261 J. Zheng, Y. Hu, J. Bai, C. Ma, J. Li, Y. Li, M. Shi, W. Tan and R. Yang, *Anal. Chem.*, 2014, **86**, 2205-2212.

## TOC graphic



This paper presents a critical review of recent research progress in plasmonic sensors, plasmon-enhanced fluorescence sensors, and surface-enhanced Raman scattering sensors. It places an emphasis on the sensor design strategies, and highlights the applications of sensors in health care, homeland security, food safety and environmental monitoring.